University of South-Eastern Norway

www.usn.no

FMH606 Master's Thesis 2024

Process Technology

Experimental and computational studies to investigate flow dynamics of Geldart A and Geldart B particles in a Circulating Fluidized Bed (CFB)

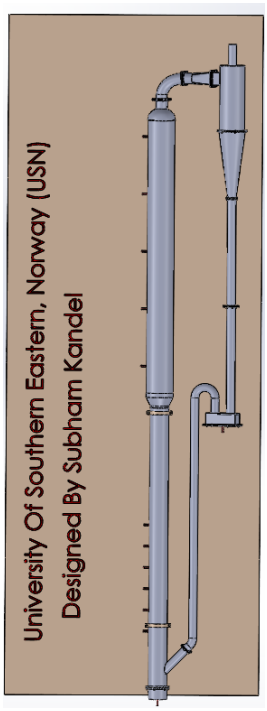

Subham Kandel

University of South-Eastern Norway

www.usn.no

Course: FMH606 Master's Thesis, 2024

Title: Experimental and computational studies to investigate flow dynamics of Geldart A and Geldart B particles in a Circulating Fluidized Bed (CFB)

Number of pages: 67

Keywords: Fluidization, Circulating fluidized bed, Barracuda, Geldart, Circulation rate, Particle size distribution, Drag model

Student: Subham Kandel

Supervisor: Prof. Britt Margrethe Emilie Moldestad, Rajan Jaiswal

External partner: Kathmandu University

University of South-Eastern Norway

www.usn.no

Summary:

In the contemporary energy landscape, the escalating demand for energy has driven efforts to develop solutions for extracting energy from renewable sources. Among various technologies, fluidized beds are notably efficient for energy extraction through biomass gasification and combustion. This efficiency is attributed to their superior mixing, enhanced heat transfer and uniform temperature distribution. CFB technology is particularly applied in processes like pyrolysis, gasification and waste firing to produce high-quality producer gas, thereby meeting emission limits. In a single reactor CFB, particles are carried by the gas flow, separated using a cyclone and returned to the riser through a gas sealing mechanism such as a loop seal or valves. The efficient design and operation of CFB reactors depend on the gas-particle flow behavior and particle circulation rate under different process conditions.

This study investigates the dynamic flow behavior of Geldart A and Geldart B particles in a CFB using both experimental and computational simulation methods. Sand particles ranging from 63-200 μm in size were used as the bed material. A CPFD model was developed using the MP-PIC approach in a Barracuda virtual reactor. The CPFD model results were validated against experimental data obtained from pressure sensor readings at different reactor zones. The optimal velocities for smooth particle circulation were identified as 1.954 m/s in the riser and 0.0531 m/s in the loop seal. The results demonstrated that the Wen-Yu Ergun drag models predicted the flow dynamics behavior closely matching the experimental measurements among the several drag models tested.

Furthermore, different simulations were conducted under various design considerations, including changes in cyclone diameter and height, the angle of the downcomer (return pipe), the height of the return pipe and the transition from a double riser to a single riser configuration. These simulations were performed using CPFD software and the impact on the particle circulation rate was observed as design changes were implemented. Finally, a new design was developed based on individual design changes that maximized the circulation rate and the percentage increase in the circulation rate was evaluated. The final design showed 20.40 % increase in circulation rate.

Acknowledgements

This thesis **"Experimental and computational studies to investigate the flow dynamics of Geldart A and Geldart B particles in a Circulating Fluidized Bed (CFB)"** was written as a part of a master's degree program at the University of South-Eastern Norway, Porsgrunn. It investigates the flow dynamics of Geldart A and Geldart B particles in different configurations of a Circulating Fluidized Bed (CFB). Through this project, I have gained good knowledge about fluidization processes, their applications and the use of CPFD software.

I extend my deepest gratitude to **Prof. Britt Margrethe Emilie Moldestad** for her guidance, continuous motivation and thorough review of my work. Prof. Britt, your encouragement and positivity, even towards my errors have been immensely inspiring and model of ideal mentorship.

I am also thankful to my co-supervisor, **Rajan Jaiswal,** for providing essential resources and assisting with experimental tasks and software simulations. Additionally, I would like to thank my external supervisor **Dr. Sunil Prasad Lohani** for his guidance and support.

Special thanks to **Niroj Koirala**, **Nirajan Raut**, **Sai Muni** and **MD Al-amin** for their continuous motivation.

Finally, I am profoundly grateful to my family and friends for their unwavering love, support and encouragement throughout this journey.

Last but not the least, I would like to thank myself for the dedication, countless sleepless nights, continuous design modifications, perseverance through simulation errors and the relentless pursuit of knowledge. This hard work has finally yielded results.

Porsgrunn, June 2024

Subham Kandel

Contents

Nomenclature

Symbol	Description	Unit
U_{mf}	Minimum fluidization velocity	m/s
U_{mb}	Minimum bubbling velocity	m/s
ΔP_b	pressure drop across bed	Pascal
ρ_p	Density of solid	kg/m^3
ρ_f	Density of fluid	kg/m^3
ε_{mf}	void fraction at minimum fluidization	-
g	gravitational force	m/s^2
d_p, d_m	Mean particle diameter	m
μ	Viscosity of gas	$kg/m\ s$
Ar	Archimedes' number	-
M	Mass of particle	kg
$U_t.$	Terminal velocity	m/s
q	Total heat transfer	J
$T_{bed,}\ T_{wall,}$	Bed temperature, wall temperature	K
h	Heat transfer coefficient	W/m^2K
L	Length of tubes	m
U_s	Particle velocity	m/s
θ_s	Particle volume fraction	-
F_P	Drag force	$kg.m/s^2$
U_f	Fluid velocity	m/s
C_d	Drag coefficient	-

List of Figure

List of Table

1 Introduction

1.1 Background

In the contemporary energy landscape, the escalating demand for energy has driven efforts to develop solutions for extracting energy from renewable sources. Among various technologies, fluidized beds are notably efficient for energy extraction through biomass gasification and combustion [1]. This efficiency is attributed to their superior mixing, enhanced heat transfer and uniform temperature distribution.

The primary product of biomass gasification in these reactors is syngas, a mixture of hydrogen (H_2), carbon monoxide (CO) and carbon dioxide (CO_2) [3]. This syngas is versatile, serving as a source for power generation, chemical synthesis and as a feedstock for synthetic fuel production. However, the utilization of fluidized bed reactors presents several challenges, including tar formation, which can cause operational issues, particle attrition and erosion that increase wear on reactor components, the complexity of reactor design and operation requiring precise control over operating conditions and the necessity for efficient ash handling systems [4]. Despite these challenges, the benefits of fluidized bed reactors, such as their ability to process diverse biomass feedstocks and their scalability, render them a promising technology for biomass gasification [5].

Fluidization is a process where solid particles in a loosely packed bed start behaving like a fluid when gas is blown upwards through them. In gas-solid system, gas is introduced at the bottom of a column containing the particles, making them vibrate and spread out to balance the drag force from the gas. As the gas speed increases, there comes a point where this drag force equals the weight of the particles, causing the bed to become fluidized [2]. Different flow patterns can form depending on the gas speed as shown in Figure 1.1.

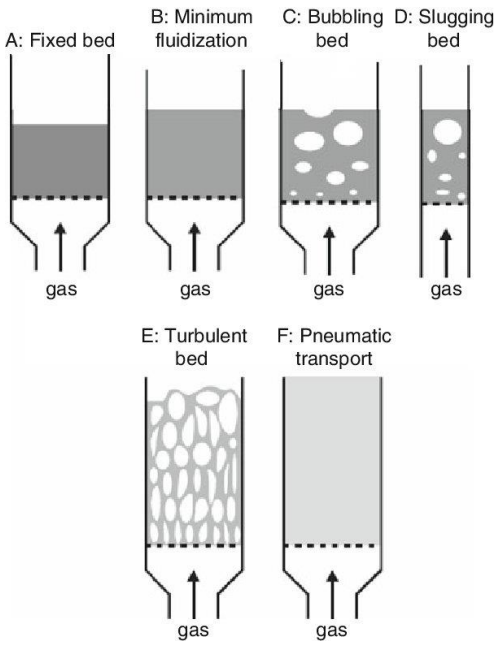

Figure 1.1 Schematic representations of fluidized beds in different regimes [22]

The regimes in fluidized beds include fixed, bubbling, slugging, turbulent and pneumatic conveying. Transition to a bubble-free fluidized bed occurs at the minimum fluidization velocity. At high gas flow rates, significant particle loss occurs due to elutriation and entrainment, mitigated by gas-solid separators. Circulating Fluidized Beds (CFBs), with higher fluid velocities enhance gas-solid contact and heat/mass transfer but are more costly due to increased power consumption and investment compared to conventional fluidized bed reactors.

The efficiency of circulating fluidized beds is highly dependent on flow behavior and understanding this behavior is crucial for scaling, designing and optimization. Over the past decades, Computational Fluid Dynamics (CFD) has become a valuable tool for predicting flow behavior in fluidized bed processes. However, further model development and validation, both of the models and the numerical methods, are still required [1].

In the work presented, minimum fluidization and pneumatic conveying parameters are determined using both experimental methods and a Computational Particle Fluid Dynamics (CPFD) model approach. The experiment used sand particles as the bed material and air as the fluidizing fluid. Sand is commonly used in fluidized bed reactors because it helps mixing the fuel with the fluidizing gas, improving mass and energy transfer. In a biomass circulating fluidized bed (CFB) reactor, biomass quickly reacts with the gas to produce synthesis gas and char. The unreacted char moves with the sand particles through the system and back to the reactor. The sand mainly controls the circulation behavior not the char [6]. Using sand in these experiments and simulations accurately reflects the flow behavior of the mixture of Geldart A and B particles in the CFB. Various design modifications are implemented on the cyclone, adjustments to the recirculating pipe inlet angle and the height of the recirculating pipe. Among the different design variants, the one exhibiting the maximum particle recirculation rate is selected and the final design is developed based on these optimized parameters. The final design is further evaluated using Barracuda Virtual Reactor 2021 to verify improvements in the particle circulation rate.

1.2 Objective

The primary objective of this study is to examine the flow dynamics of Geldart A and Geldart B particles within a Circulating Fluidized Bed (CFB). To achieve this, a series of experimental and simulation tasks will be undertaken:

Experimental Tasks:

1. Conduct experiments on the CFB at various gas velocities.
2. Characterize the properties of the particles used.
3. Measure the entrained mass of particles over a one-hour duration.
4. Monitor the pressure variation along the reactor during fluidization using LabView.

Simulation Tasks:

1. Create a CAD model of the experimental CFB setup available at USN.
2. Develop and validate a CPFD model of the CFB using Barracuda Virtual Reactor software, aligning it with the experimental data.
3. Analyze the impact of design parameters on particle circulation rates and fluid dynamics behavior.
4. Develop a final design incorporating all the best part design from individual design modifications.
5. Perform post-processing of the CPFD model results to identify:
    - The rapid fluidization regime and particle distribution within the bed.
    - Particle circulation patterns.
    - Pneumatic conveying rates of the particles.
    - Flow dynamics behavior of the CFB under various operating conditions.

1.3 Thesis Outline:

This thesis is structured into seven chapters: Chapter 1 introduces the background, objectives and an overview of the study. Chapter 2 provides a literature review on fluidization regimes, particle classification and a brief introduction to circulating fluidized beds. Chapter 3 outlines the methodology, detailing both the experimental and simulation procedures. Chapter 4 presents the results and discussion including model validation and the impact of various design modifications on particle circulation rates. Chapter 5 summarizes the work and concludes the report. Chapter 6 includes the references consulted and Chapter 7 contains the appendices.

2 Literature Review

Several factors influence the fluidization process, including fundamental parameters such as particle size, shape and density as well as the design of the fluidized bed itself. Both aspects are crucial for accurately calculating and predicting the dynamic behavior within fluidized beds [10]. Among the various software's available for predicting fluidization, Computational Particle Fluid Dynamics (CPFD) is notable and is used in the further design modifications. Fluidization can occur with either a gas or a liquid in a bed of particles, however this thesis focuses exclusively on gas-solid fluidization. This chapter provides a literature review of fluidization concentrating on topics relevant to this work.

2.1 Review of Fluidization Basics

Fluidization is a process where solids behave like a fluid by blowing gas or liquid upwards through a reactor filled with solid particles [10]. This technique is widely used in commercial operations and can be categorized into two main types:

Physical operations such as heating, absorption and mixing of fine powders.

Chemical operations including reactions of gases on solid catalysts and reactions of solids with gases.

The fluidized bed is one of the most well-known methods in the processing industry. Its key advantages include excellent particle mixing leading to low temperature gradients, suitability for both small and large-scale operations and the capability for continuous processing. Many established processes utilize this technology such as coal carbonization and gasification, ore roasting and coating preparations [30].

2.2 Geldart's Classification of Particles

Not all particles can be fluidized. The fluidization behavior of solid particles primarily depends on their size and density. Geldart's observation, illustrated in Figure 2.1, categorizes the characteristics of four distinct types of particles as follows:

Group A is designated as 'aeratable' particles. These particles have small mean particle size (d_p< 150 µm) and/or low particle density (<~1.4 g/cm^3). These solids fluidize easily, with smooth fluidization at low gas velocities without the formation of bubbles. At higher gas velocity a point is eventually reached when bubbles start to form and the minimum bubbling velocity U_{mb} is always greater than U_{mf} [11].

Group B is called 'sand like' particles or bubbly particles. Most particles of this group have size 150 µm to 500 µm and density from 1.4 to 4 g/cm^3. For these particles, once the minimum fluidization velocity is exceeded, the excess gas appears in the form of bubbles. Bubbles in a bed of group B particles can grow to a large size. Typically used group B materials are glass beads and coarse sand [11].

Group C materials are ‘cohesive’, or very fine powders. Their sizes are usually less than 30 μm and they are extremely difficult to fluidize because interparticle forces are relatively large compared to those resulting from the action of gas. In small diameter beds, group C particles easily give rise to channeling. Examples of group C materials are talc, flour and starch [11].

Group D is called ‘spoutable’ and the materials are either very large or very dense. They are difficult to fluidize in deep beds. Unlike group B particles as velocity increases, a jet can be formed in the bed and material may then be blown out with the jet in a spouting motion. If the gas distribution is uneven, spouting behavior and severe channeling can be expected. Roasted coffee beans, lead shot and some roasted metal ores are examples of group D materials [11].

Geldart’s classification is clear and easy to use as displayed in Figure 2.1 for fluidization at ambient conditions and for U less than about 10*U_{mf} [4]. For any solid of a known density ρ_s and mean particle size d_p this graph shows the type of fluidization to be expected. It also helps predicting other properties such as bubble size, bubble velocity, the existence of slugs etc.

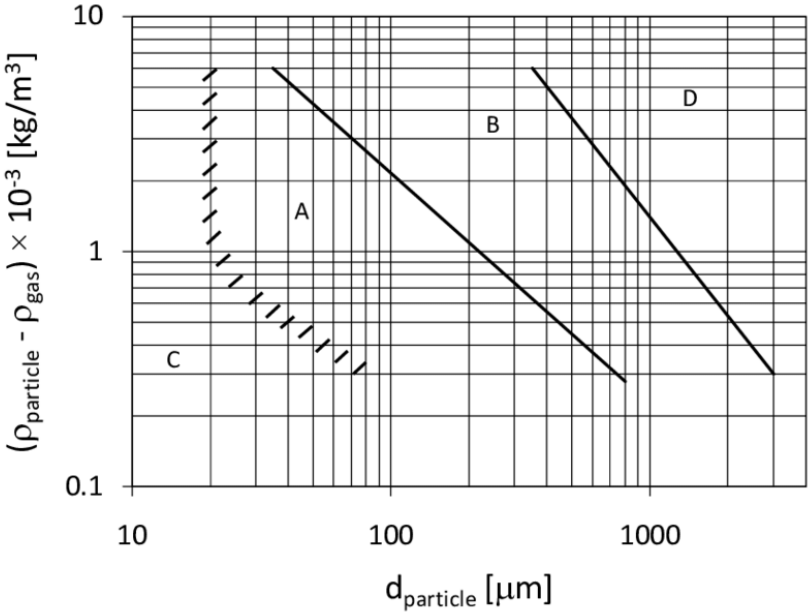

Figure 2.1 Diagram of the Geldart classification of particles [11]

Various types of patterns can be seen when we look at the bubble rise in Geldart A, B, C and D particles (Figure 2.2). Small and large bubbles are observed in A and B whereas channeling and spouting are observed in C and D.

Channeling is an abnormality of fluidized bed where the gas flows through one or two specific preferred paths. Channeling is greatly affected by particle size, density and particle size distribution. Solids with high moisture content or high bed viscosity tends to form clumps known as snowballs which then enhances the formation of channels in the bed [28]. During channeling a large portion of bed remains static while fluid by passes through the channels. This results in inefficient mixing and reduced contact between the fluid and the particles.

Sprouting, also known as jetting occurs when fluid shoots up through the bed in narrow, concentrated stream similar to jet causing particles to be ejected upwards. Sprouting disrupts the uniform fluidization and can cause uneven particle distribution in a mixture of particles [29].

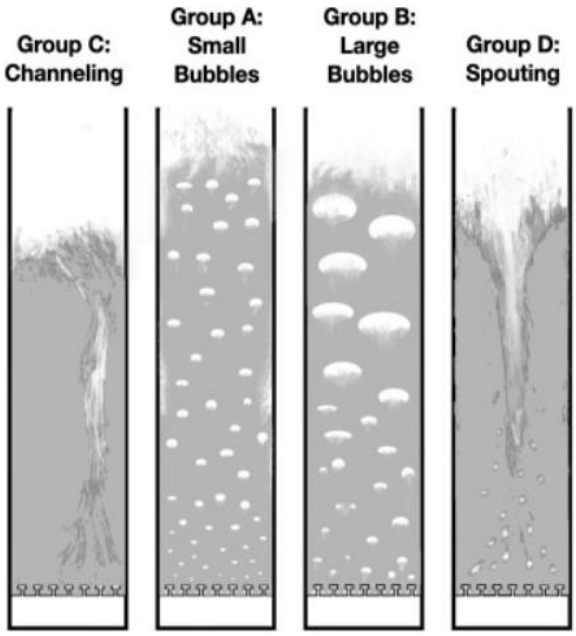

Figure 2.2 Fluidization behavior [19]

2.3 Fluidization Regime

When solid particles are fluidized, the behavior of the fluidized bed changes with variations in velocity and properties of the gas and solids [23]. There are several fluidization regimes, as illustrated in Figure 2.3.

Fixed Bed (Figure 2.3A): At low gas flow, particles vibrate but remain at the same height as the bed at rest.

Minimum Fluidization (Figure 2.3B): As gas velocity increases, the drag force from the gas equals the weight of the particles, causing slight bed expansion. This point is the onset of fluidization, characterized by the minimum fluidization velocity (U_{mf}).

Bubbling Fluidized Bed (Figure 2.3C): Further increasing the gas flow forms fluidization bubbles, leading to a bubbling fluidized bed.

Slugging (Figure 2.3D): At higher velocities, bubbles in the bed coalesce and grow as they rise. If the bed's height to diameter ratio is high, bubble size can match the bed diameter.

Turbulent Bed (Figure 2.3E): At very high gas flow rates, the velocity exceeds the particle's terminal velocity, causing turbulent motion of solid clusters and gas voids. The upper bed surface disappears, replaced by this turbulent mixture.

Entrained Bed: With even higher gas velocities, the bed transitions to an entrained bed, resulting in a disperse, dilute or lean phase fluidized bed, resembling pneumatic transport of solids.

Each regime represents a distinct phase of fluidization behavior as the gas velocity increases.

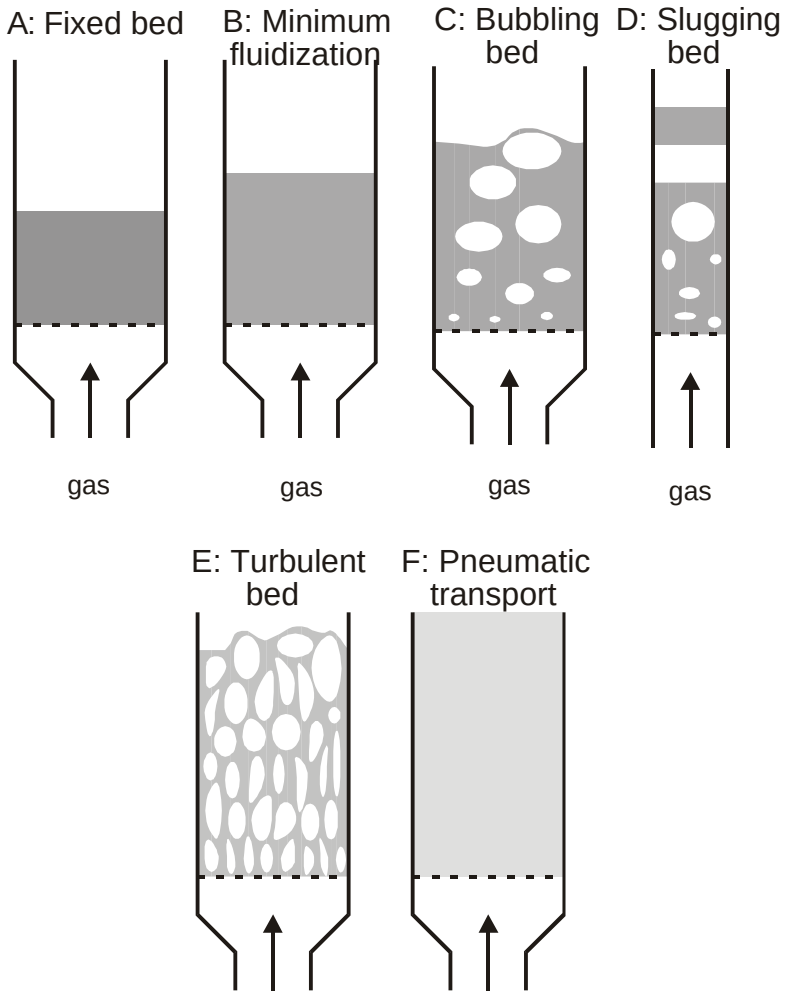

Figure 2.3 Schematic representation of fluidized beds in different regimes [22]

2.3.1 Packed Beds

When talking about packed beds, the solid particles are in dense phase and gas is passed continuously through the bed of particles. In this regime, the drag force is less than the gravitational force and the particles will be in a stationary condition. As the flow rate of the gas is incrementally increased, an initial response is observed where certain particles may begin to oscillate or vibrate slightly due to the localized disturbances in the gas flow [30]. Despite this agitation, the overall bed height does not change, reflecting that the bulk of the particles are still not experiencing sufficient lift to initiate significant movement or expansion of the bed.

2.3.2 Bubbling Fluidized Bed

A fluidized bed is mostly referred to as bubbling fluidized bed type as shown in Figure 2.3C. Gas fluidized beds are characterized by the 'bubbles' which is formed at superficial gas velocities higher than that required to just fluidize the particles. This type of fluidization has been called 'aggregative fluidization', and under these conditions, the bed appears to be divided into two phases, the bubble phase and the emulsion phase. The bubbles appear to be very similar to gas bubbles formed in a liquid and they behave in a similar manner. The bubbles coalesce as they rise through the bed [9].

The movement of particles in fluidized beds is largely dependent on bubbles rising through the bed. Therefore, special attention should be paid to bubbles and their properties [6]. To give an impression of the processes occurring inside a fluidized bed reactor, the principles of fluidization, the formation of bubbles, their path through the bed, the way they transport particles concerning gas fluidized bed and important parameters are described below.

2.3.2.1 Minimum Fluidization Velocity

The superficial gas velocity at which the bed of particle is just fluidized is called the minimum fluidization velocity and designated by U_{mf}[10].

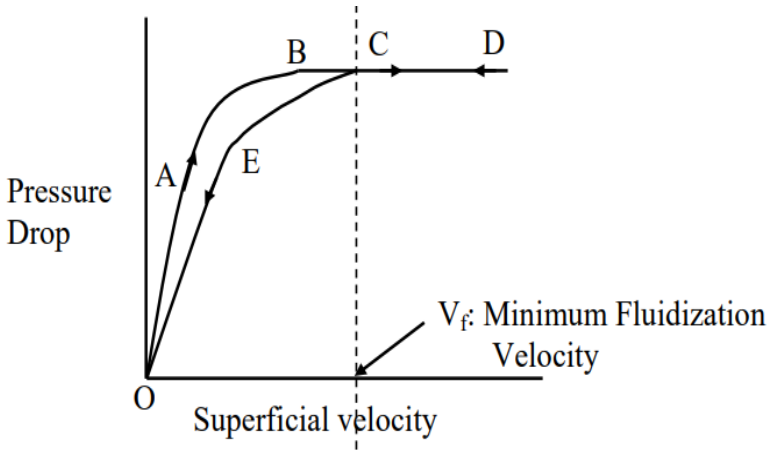

Figure 2.4 Pressure Drop VS Superficial Velocity [23]

At this state, the drag force exerted on a particle is equal to its net weight. As far as the whole bed is concerned, the drag force can be calculated from the product of bed pressure drop (ΔP_{mf}) and the cross-sectional area (A) of bed [23]. So,

$$F = \Delta P_{mf} A \qquad 2.1$$

Also, the net bed weight is the product of the bed volume ($V_{mf} = A\ l_{mf}$), net density ($\rho_s - \rho_f$), the fraction of the bed ($1 - \varepsilon_{mf}$)), which is occupied by the particles.

$\Delta P_{mf} A = A.\, l_{mf}(\rho_s - \rho_f)(1 - \varepsilon_{mf})g$

$\Delta P_{mf} = l_{mf}(\rho_s - \rho_f)(1 - \varepsilon_{mf})g$ 2.2

So, at minimum fluidization velocity the density of the fluidized solids is equal to the difference between particle density and fluid density. The fraction of the bed $(1 - \varepsilon_{mf})$ occupied by the particles is used because only the particles contribute significantly to the pressure drop. The superficial gas velocity and consequent pressure drop relationship help to predict MFV. But modeling this relationship is difficult because of the irregular shape of particles, void spaces and twisting flow path of the fluid [13].

For isotropic-shaped solids:

$$\frac{1.75}{\epsilon_{mf}^3 \emptyset_s}\left(\frac{d_p U_{mf} \rho_g}{\mu}\right)^2 + \frac{150(1-\varepsilon_{mf})}{\epsilon_{mf}^3 \emptyset_s^2}\left(\frac{d_p U_{mf} \rho_g}{\mu}\right) = \frac{d_p^3 \rho_g (\rho_s - \rho_g) g}{\mu^2} \qquad 2.3$$

$$\frac{1.75}{\epsilon_{mf}^3 \emptyset_s} Re_{mf}^2 + \frac{150(1-\varepsilon_{mf})}{\epsilon_{mf}^3 \emptyset_s^2} Re_{mf} = Ar \qquad 2.4$$

where Ar is Archimedes number.

In solving the Equation, U_{mf} can be calculated by

$$U_{mf} = \frac{d_p^2(\rho_s - \rho_g)g}{150\mu}\frac{\epsilon_{mf}^3 \emptyset_s^2}{1-\varepsilon_{mf}} \qquad Re_{mf} < 20 \qquad 2.5$$

$$U_{mf}^2 = \frac{d_p^2(\rho_s - \rho_g)g}{150\mu}\varepsilon_{mf}^3 \emptyset_s \qquad Re_{mf} > 1000 \qquad 2.6$$

The Equation can be re-arranged as

$$K_1 Re_{mf}^2 + K_1 Re_{mf} = Ar \qquad 2.7$$

where, $K_1 = \frac{1.75}{\epsilon_{mf}^3 \emptyset_s}$ and $K_2 = \frac{150(1-\varepsilon_{mf})}{\epsilon_{mf}^3 \emptyset_s^2}$

Many studies have been conducted to find the minimum fluidization velocity and the correlation for different Geldart groups is tabulated below.

Table 2.1 Correlation for U_{mf} for different particle sizes, densities and Geldart Groups

Authors	Correlation	Particle diameter [μ_m]	Particle density [kg/m^2]	Geldart groups
Wen and Yu	Re_{mf} = $(33.7^2 + 0.0408\text{Ar})^{0.5} - 33.7$	2052-6350	2360-7840	D
Bourgeis and Grenier	Re_{mf} = $(22.56^2 + 0.0382\text{Ar})^{0.5} - 25.46$	86-25000	1200-19300	A, B, D
Saxena and Vogel	Re_{mf} = $(25.28^2 + 0.0571\text{Ar})^{0.5} - 25.28$	650 – 704	1900-2460	B, D
Babu, Shah and Talwalker	Re_{mf} = $(25.25^2 + 0.0651\text{Ar})^{0.5} - 25.25$	50 – 2870	2560-3920	A, B, D
Vaid and Sen Gupta	Re_{mf} = $(24^2 + 0.0546\text{Ar})^{0.5} - 24$	114 – 1829	1669 - 4332	B, D
Chitester, Kornosky, Fan, Danko	Re_{mf} = $(28.7^2 + 0.0494\text{Ar})^{0.5} - 28.7$	88 – 374	1.12 – 2.47	A, B

2.3.2.2 Bubble Size

The mean size of the bubble population in fluidized beds increases with height above the distributor plate due to coalescence of bubbles. Researchers have attempted to predict the size of bubbles, not only the variation in mean size but also the distributions of the diameter and volume [23].

As far as the mean size is concerned, Geldart used the expression of Kato and Wen for the initial bubble size at the gas distributor. He asserted that a porous plate distributor behaves as a distributor plate with 1 hole per 10cm^2 and added his own empirical expression for the bubble growth with bed height due to coalescence [11].

$$\text{DB}= \frac{1.43}{g^{0.2}}\left(\frac{(U-U_{mf})\pi \text{D}_{bed}{}^2}{4No}\right)^{0.4} + 2.05(U-U_{mf})^{0.94}h \qquad 2.8$$

where DB is the bubble diameter, D_{bed} is the diameter of the bed and No is the number of holes in the distributor plate.

2.3.2.3 Bubble Wake:

When a bubble rises, it carries some amount of solids inside as seen in Figure 2.5. This is called ‘wake’. The formation of a wake follows directly when the bubble forms. Hence, the bubble

picks up most of its solids at the bottom of the bed as it leaves the distributor plate [9]. An idealized bubble has an upper surface that is approximately spherical with a radius of curvature r and a wake at the bottom with wake angle $\theta_w$as shown in Figure 2.5.

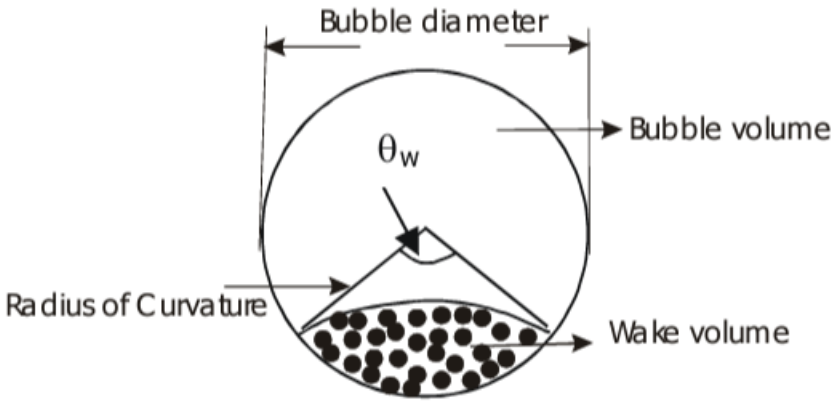

Figure 2.5 Bubble Wake on a bubble

The bubble size is often expressed in terms of the volume equivalent diameter D_{eq}, and can be calculated as

$D_{eq} = (\frac{6Vb}{\pi})^{\frac{1}{3}}$ where Vb is a bubble volume.

2.3.2.4 Bubble Rise Velocity:

The rise velocity of a large spherical cap bubble in a liquid is dependent on the radius of curvature at the nose of the bubble as described [21]

$$U_b = 0.667\sqrt{g.r} \qquad 2.9$$

A semi-empirical relation in terms of the volume-equivalent diameter is

$$U_b = 0.711\sqrt{g.D_{eq}} \qquad 2.10$$

where $U_b\ is$ bubble rise velocity, g is accleration due to gravity and r is the radius

2.3.3 Slugging Regime

When the superficial gas velocity is increased further, the bubbles become larger due to collision and therefore occupy the bed diameter. This phenomenon is called slugging and the velocity at onset of slugging is known as minimum slugging velocity [18]. According to Stewart and Davidson [23] the minimum slugging velocity can be expressed as

$$U_{ms} = U_{mf} + 0.07\sqrt{gD} \qquad 2.11$$

Where U_{ms} is minimum slugging velocity, U_{mf} is mimimum fluidization velocity, g is accleration due to gravity and D is the diameter.

Formation of slugs depends on the bed aspect ratio. In a large-diameter bed, slugs rarely occur because the bubbles will not be able to grow up to the bed diameter. If the bed materials are fine particle size, it makes it difficult to slug [23]. The gas-solid interaction in a fluidized bed is highly influenced by the bubbling and slugging regimes. Therefore, it is important to determine the onset of bubbling and slugging regimes and their transition, when designing the fluidized bed reactor [14].

2.3.4 Turbulent Regime

On increasing the superficial velocity, the solid particles become vigorous and travel very fast from the riser. When the superficial velocity is increased further, bubble formation starts to break, the pressure fluctuation gradually decreases and becomes stable [19]. Due to this, the bed expands and the particles are thrown above the bed. Yerushalmi and Cankurt characterized this transition in terms of two velocities, namely u_c at which the pressure fluctuations peak, and $U_k$where the pressure fluctuations begin to level off.

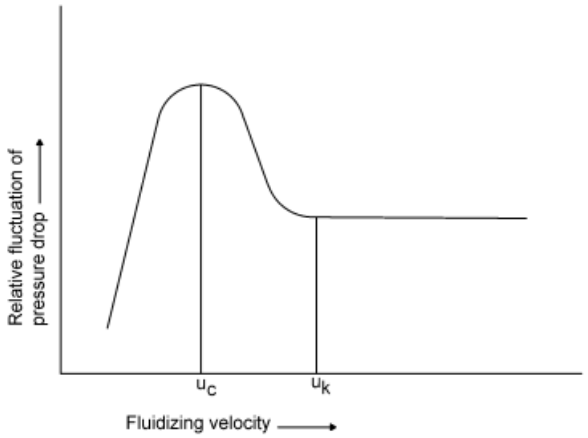

Figure 2.6 Relative fluctuation of pressure drop vs velocity [19]

The correlations for the small diameter beds proposed by Grace:

$$u_c = 3.0\sqrt{\rho_p d_p} - 0.17 \quad 2.12$$

$$u_k = 7.0\sqrt{\rho_p d_p} - 0.77 \quad 2.13$$

$$\rho_p d_p = 0.05 - 0.7\ kg/m^2 \quad 2.14$$

$$Re_c = \frac{u_c d_p \rho_g}{\mu} = 0.936Ar^{0.472} \quad (2.15)$$

$$Re_k = \frac{u_k d_p \rho_g}{\mu} = 1.46Ar^{0.472} \quad (Ar < 10^4) \quad (2.16)$$

$$= 1.46Ar^{0.56} \quad (Ar > 10^4)$$

The turbulent fluidization can occur above the terminal velocity for the fine particles and for the coarse particles it can be below the terminal velocity [19].

2.3.5 Fast Fluidization

When the superficial gas velocity is increased beyond the turbulent velocity, the solid particles will travel in an upward direction and will be released into the environment. Therefore, the circulating fluidized bed is used for the re-circulation of solid particles. The fundamental design and operation of CFB is discussed in Figure 2.7. The main features of these regimes are high slip velocity between gas and solid, particle agglomerate and good particle mixing [17]. Figure 2.7 below describes the solid particle circulation as the dense particles are moving downwards and the light particles are moving in an upward direction.

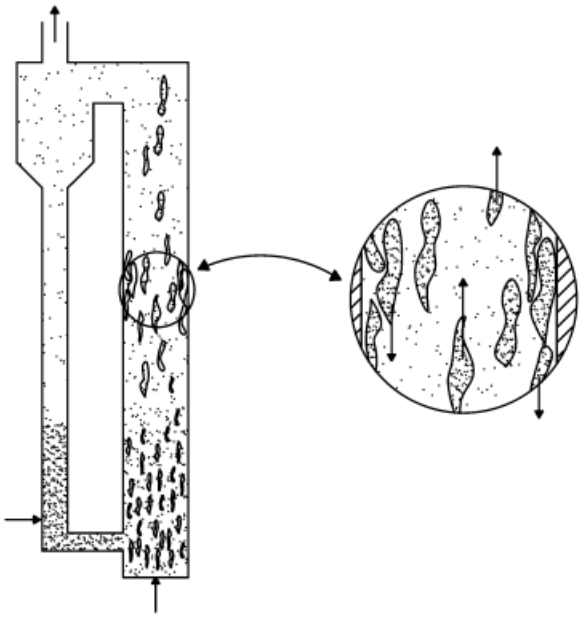

Figure 2.7 Solid Particle Recirculating

2.3.6 Pneumatic Transport

The solid particles are transported to the cyclone and back to the riser through a loop seal. This regime is considered the final stage of regimes in fluidization and the average pressure drop across the reactor height is minimal. The superficial gas velocity for the circulation of solid particles can be verified only in experiments as there is no such correlation to find the pneumatic transport velocity [10].

2.4 Flow Pattern of Fluidization Bubbles

As bubbles rise through the bed, they coalesce to form bigger bubbles and when they become too large, they split. The average bubble size equilibrates at about the maximum stable size. The location in the bed where the equilibrium size is attained depends on the kind of particles [30]. For group A particles, the maximum stable diameter is relatively small therefore the average bubble size stabilizes close to the distributor plate and remains constant through the rest of the bed. The maximum stable diameter for group B particles is larger and the equilibrium is reached typically only in the upper levels of the bed. The bubbles in group D particle beds behave differently, they do not rise as individual bubbles but as horizontally associated swarms [12].

Bubbles can coalesce in two ways, by incorporating a bubble in front or by moving side-wards into the track of another bubble and then incorporating it. At the wall of the bed, bubbles can only move inwards, while other bubbles can move in any horizontal direction. The result is an active zone away from the wall, which intensifies and moves closer to the axis with increasing distance from the distributor plate. Solid particles are dragged up by the bubbles and by continuity, will move downwards in regions with lower bubble densities. As a consequence of fewer bubbles being close to the wall, there is a predominantly downward flow of particles near the wall which once established, maintains the tendency for bubbles to move inwards. The overall circulation is upwards near the axis and downwards near the wall in higher regions and the converse seems to be the case in the lower regions [18].

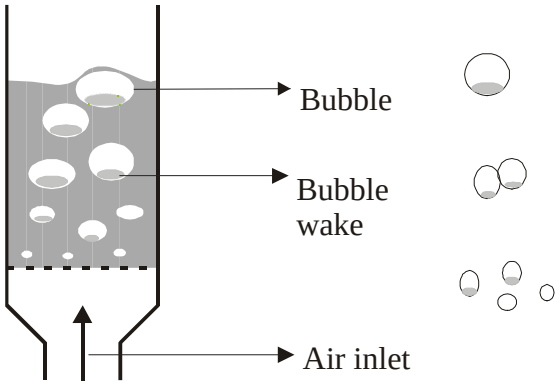

Figure 2.8 Bubble wake in a Bubbling Fluidized Bed

2.5 Circulating Fluidized Bed

Solid particles are often of great interest in the chemical processing industry, mineral processing, pharmaceutical production, energy-related processes etc. In some cases, the particles serve as catalysts for reacting gases or liquids. In other cases, as in ore processing, the particles must be chemically converted. In still other processes the particles must undergo physical transformation as in drying of particulate solids [17].

A number of possible configurations are available for carrying out such reactions and contacting operations. For example in industrial calcination and combustion processes, there are competing technologies based on fixed, fluidized beds and dilute-phase transport systems [16]. The circulating fluidized bed (CFB) has come to prominence in the past two decades in terms of major applications. A typical configuration for a CFB reactor is shown schematically in Figure 2.9.

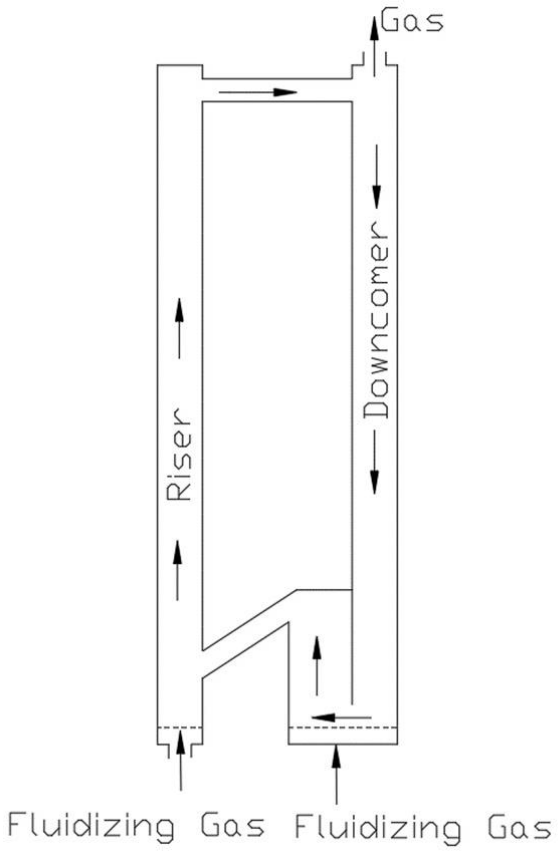

Figure 2.9 Typical Configuration of Circulating Fluidized Bed System

For a circulating fluidized bed, it is essential to have a tall vessel, a mechanism for introducing particles typically near the bottom, an adequate upwards flow of fluid (gas or liquid) to achieve substantial entrainment of particles from the top of the vessel and a method for capturing a substantial majority of these particles and continuously returning them to the bottom. The term "circulating" signifies that the particle separation and return systems are integral and essential components of the overall reactor configuration. The word 'fluidized bed' denotes the fact that the particles are supported by the fluid, while there is still a substantial suspension density. Note that there is unlikely to be a true 'bed' in the normal sense, in particular most circulating fluidized beds operate in the 'fast fluidization' hydrodynamic regime where there is no distinct or recognizable upper bed surface [16].

A gas-solid two-phase vertical flow system without mechanical restraint can be operated in three modes, co-current up flow, co-current downflow and counter-current flow with gas flowing upward as shown in Figure 2.10.

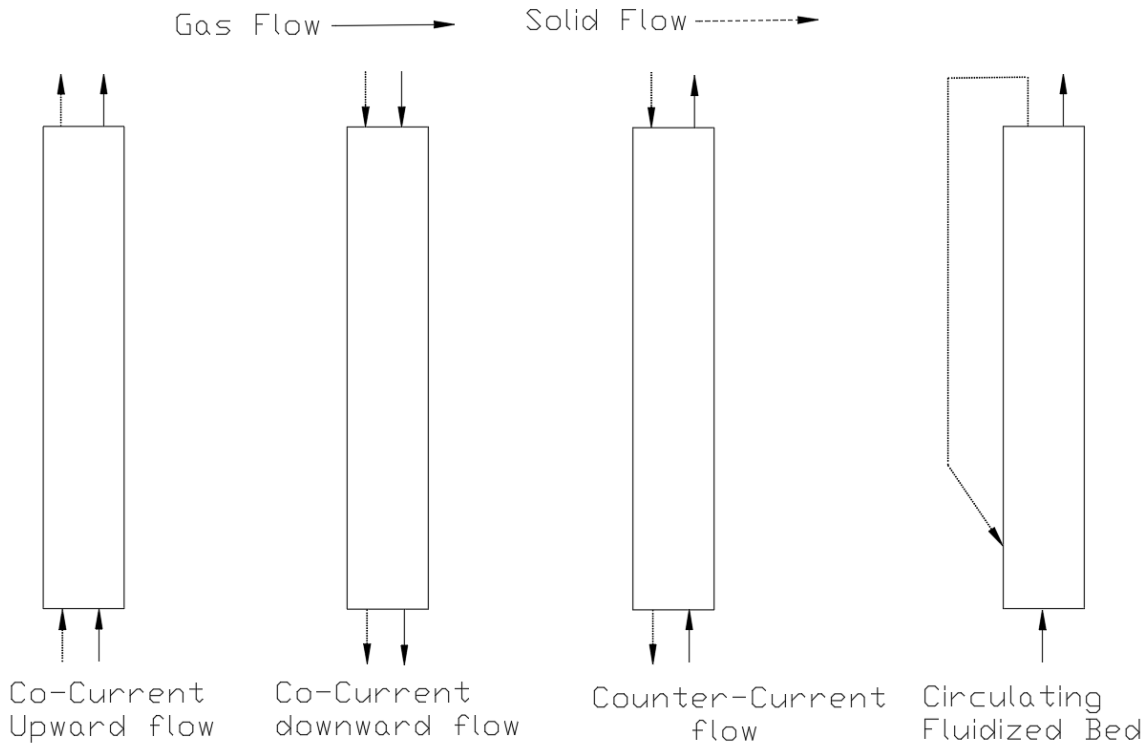

Figure 2.10 Flow mode of gas-solids vertical flow system [28].

2.5.1 Advantages and disadvantages of CFB systems

Circulating fluidized beds offer several advantages that make them superior to traditional low velocity fluidized beds. Firstly, they provide improved gas-solid contacting due to the absence of bubbles, ensuring more efficient interactions between the gas and solid particles. Additionally, the higher superficial velocity in these systems allows for a reduced cross-sectional area making them more space efficient. Unlike low-velocity beds, circulating fluidized beds do not have a freeboard region where significant temperature gradients can occur, resulting in more uniform temperature distribution throughout the system. This design also reduces the tendency for particle agglomeration, maintaining the fluidization quality. Finally, they offer greater operating flexibility, allowing for a wider range of operational conditions and adjustments [23].

Despite their many advantages, circulating fluidized beds come with several disadvantages. One of the primary drawbacks is the increased overall reactor height, which can pose significant design and installation challenges. This taller design, combined with the complexity of the recirculating loop, leads to higher capital costs. Additionally, the design and operation of the recirculating loop add further complexity, requiring more sophisticated control and

monitoring systems. Another issue is increased particle attrition, which can lead to higher wear and tear on the equipment and the need for more frequent maintenance or replacement of the particles. These factors collectively contribute to the higher cost and operational demands of circulating fluidized beds [23].

2.6 Components of Circulating Fluidized Bed

The components of Circulating fluidized are

1. Cyclone
2. Riser
3. Stand pipe
4. Loop seal
5. Return Pipe / Downcomer

2.6.1 Riser:

The riser is the main component of a circulating fluidized bed where solid particles are kept at first. Gas passes from the bottom of the riser, to fluidize the system. The particles then start to move and eventually reach the cyclone, loop seal and move back to the riser.

2.6.2 Cyclone:

A cyclone is a device that separates particulate solids from a fluid stream by a radial centrifugal force exerted on the particles. This force separates the solid from the gas by driving the solids to the cyclone wall, where they slide down to the bottom outlet and are collected. Cyclones are widely used in conjunction with fluidized beds to remove solids from exit gas stream [16]. Cyclones have no moving parts, are relatively inexpensive to construct and maintenance cost are low.

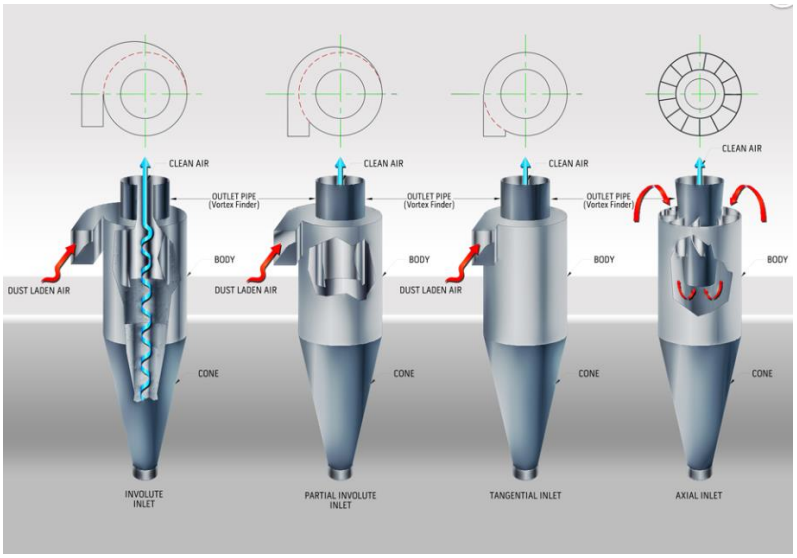

Figure 2.11 Different Inlet Positions in a Cyclone

Depending upon the inlet position, different confriguation of cyclone are present which is shown in Figure 2.11.

There are many parameters that affect the collection efficiency of a cyclone. Among them the height and diameter of cyclone have a major role.

2.6.2.1 Changing diameter keeping height constant.

Changing the diameter of a cyclone in a circulating fluidized bed (CFB) system can have several effects on its effectiveness.

- Centrifugal Force and Collection Efficiency:

The primary mechanism of particle separation in a cyclone is the centrifugal force that acts on particles as the gas stream spirals down the cyclone. This force is inversely proportional to the cyclone's diameter [24]

$$F_c = \frac{mv^2}{r}$$

Where F_c is the centrifugal force, m is the particle mass, v is the tangential velocity and r is the radius.

Increasing the diameter (d) increases r, reducing the centrifugal force and thus the efficiency of particle separation.

- Cut Size:

The cut size (d_{50}) is the particle size at which the cyclone collects 50% of the particles [24].

$$d_{50} \propto \sqrt{\frac{d}{\Delta p}}$$

where d is the cyclone diameter and Δp is the pressure drop.

As the diameter increases, the cut size increases meaning the cyclone becomes less effective at capturing smaller particles [24].

- Pressure Drop:

The pressure drop across a cyclone is related to its size and design [25]

$$\Delta p \propto \sqrt{\frac{\rho v^2}{2}}$$

where ρ is the gas density and v is the velocity. Increasing the diameter typically reduces the gas velocity for a given volumetric flow rate, leading to a lower pressure drop [25].

- Residence Time:

Residence time is the time the gas stream spends inside the cyclone [13]. Increasing the diameter increases the residence time, which might seem beneficial, but it also means lower velocities and weaker centrifugal forces.

2.6.2.2 Changing the Height of Cyclone keeping Diameter Constant.

There are various effects on particle recirculation rate while changing the height of cyclone keeping diameter constant.

- Gas and Particle Residence Time:

Increasing the height of the cyclone generally increases the residence time of the gas and particles within the cyclone. This longer residence time allows more opportunity for particles to be separated from the gas stream by centrifugal forces [16].

- Improved Separation**:**

A taller cyclone can enhance separation efficiency because particles have more time to move towards the cyclone walls under the influence of centrifugal forces. This can result in a higher probability of particle capture. The enhanced particle capture reduces particle losses and ensures more consistent particle reintroduction into the CFB system, contributing to better operational stability and efficiency [24].

- Velocity Profile**:**

The height of the cyclone affects the velocity profile of the gas stream. A taller cyclone can help maintain a more stable and favorable velocity gradient for particle separation [24].

2.6.3 Angle of recirculation pipe (Return leg or downcomer)

- Increased Angle (Steeper Recirculating Pipe):

Enhanced Particle Flow: A steeper angle (closer to vertical) improves the gravitational force assisting particle movement. This enhances the particle recirculation rate as particles flow more smoothly and quickly back to the reactor.

Reduced Blockages: The risk of blockages decreases with a steeper angle because particles are less likely to settle and accumulate within the pipe.

- Decreased Angle (Shallower Recirculating Pipe):

Reduced Particle Flow: A shallower angle (more horizontal) reduces the gravitational assistance, potentially leading to slower particle movement and a reduced recirculation rate.

Increased Blockages: The likelihood of particle settling, and blockages increases with a shallower angle, disrupting the consistent return of particles to the reactor and potentially affecting the system's overall efficiency.

2.6.4 Length and Height of Recirculating pipe.

After the particles move from loop seal, it comes to the riser via recirculating pipe. The length of the recirculating pipe has a great impact on circulation rate. The greater the length of recirculating pipe after the loop seal, the more the particles get accumulated and the flow gets disturbed. But as soon as the loop seal and standpipe accumulate enough pressure, recirculation starts. Maintaining good height of recirculating pipe helps in good recirculation rate.

2.7 Heat Transfer

The heat transfer rate is essential for combustion or any exothermic reaction processes in CFB. Heat transfer coefficient, h is used to determine the heat transfer rate. The heat transfer in CFB can be expressed as:

$$q = hA(T_{bed} - T_{wall}) \qquad 2.17$$

The value of h is influenced by the cross-sectional average solid's density and the elevated temperature. The hydrodynamics of the gas-solid mixture near the wall affects the process of heat transfer [34]. The clusters of particles or individual particles are moved in an upward direction at a certain velocity and circulate at a uniform temperature. On decreasing velocity, the particles tend to fall downward. The relative time of cluster-wall contact and the thermal time constant of the particle are used to determine the good heat transfer rate. If the cluster stays on the wall for a long period of time, heat transfer from the particles is reduced.

The cluster (collection of particles) is not stable. The three different modes of heat transfer are conduction (dispersed phase), convection (cluster phase) and radiation (both).

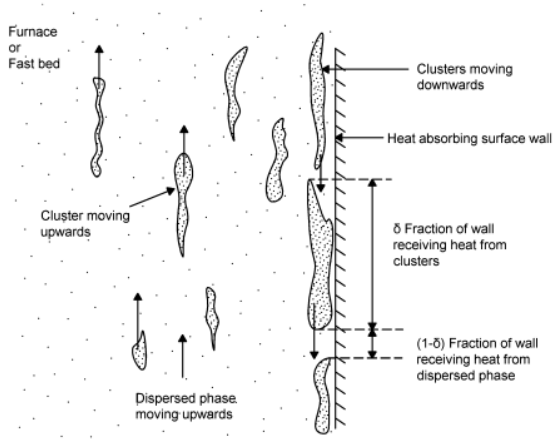

Figure 2.12 Mechanism of heat transfer [34]

2.8 Solids Mixing

The flow dynamics of the CFB system falls on the fast fluidization regime. The particles move up and down direction in the riser resulting increase in the residence time for mixing and are used to develop the physical properties of solid particles. For the exothermic reactions, the

solid particles must be mixed properly to avoid the hot spots. With respect to solid volume concentration, the riser can be categorized into 4 zones as in Figure 2.13.

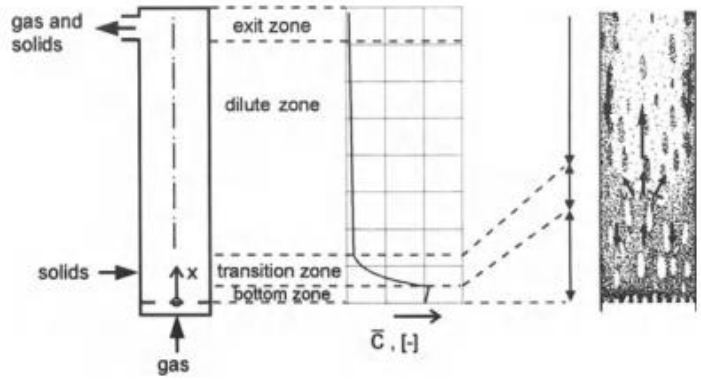

Figure 2.13 Different zones of riser in CFB [34]

2.8.1 Particle motion in the bottom zone

According to Svensson et al., the lower zone behaves as a bubbling or turbulent fluidized bed based on the pressure fluctuation data. The particles are stored in the bottom zone on passing the air from distributor plate attached below the riser, the particles start to break and then fed to the transition zone.

2.8.2 Particle motion in the transition zone

The particle from the dense bottom zone is carried to the dilute zone and the clusters moved back to the bottom zone due to gas velocity and particle size. Therefore, high intensity of solids mixing occurs in this zone.

2.8.3 Particle motion in the dilute zone

In this zone the riser is distinguished into two phases, lean phase and dense phase. In the lean phase, the particle moves upward and in dense phase the particle travel downward back to the lower zone. The solid concentrations are higher in dense phase than lean phase.

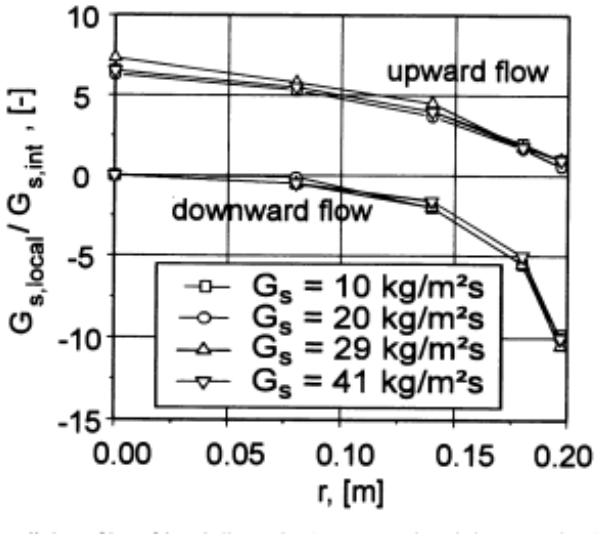

Figure 2.14 Solid mass flux in dilute zone [34]

The solid mass flux in lean phase reaches maximum at the center of the riser and then decreases near the wall, while in the dilute phase it is the opposite.

2.8.4 Particle motion in the exit zone

The particles are then pushed to the cyclone where the gas and solids are separated. The lighter particles elutriated along with the gas and the heavier particles traveled back to the riser (lower zone) through loop seal.

2.9 Importance of Barracuda

Modeling gas-solid flow behavior is complex due to gas flow, particle movements and inter-particle collisions. There are two basic modeling approaches, Lagrangian-Eulerian and Eulerian-Eulerian. Lagrangian-Eulerian modeling tracks each particle individually using Newton's laws, while the gas phase is modeled with Navier-Stokes Equations [31]. Eulerian-Eulerian modeling treats both phases as continuous and uses Navier-Stokes Equations for both, requiring more closure functions but less computational power. However, Lagrangian-Eulerian simulations while precise demand significant computational resources, making them impractical for industrial applications [32]. The Multiphase Particle in Cell (MP-PIC) method, an extension of Lagrangian-Eulerian models group particles (parcels) instead of individual particles, balancing discrete and continuous modeling [33]. MP-PIC is integrated into the Barracuda VR software, popular for computational particle fluid dynamics (CPFD) [20].

3 Methodology

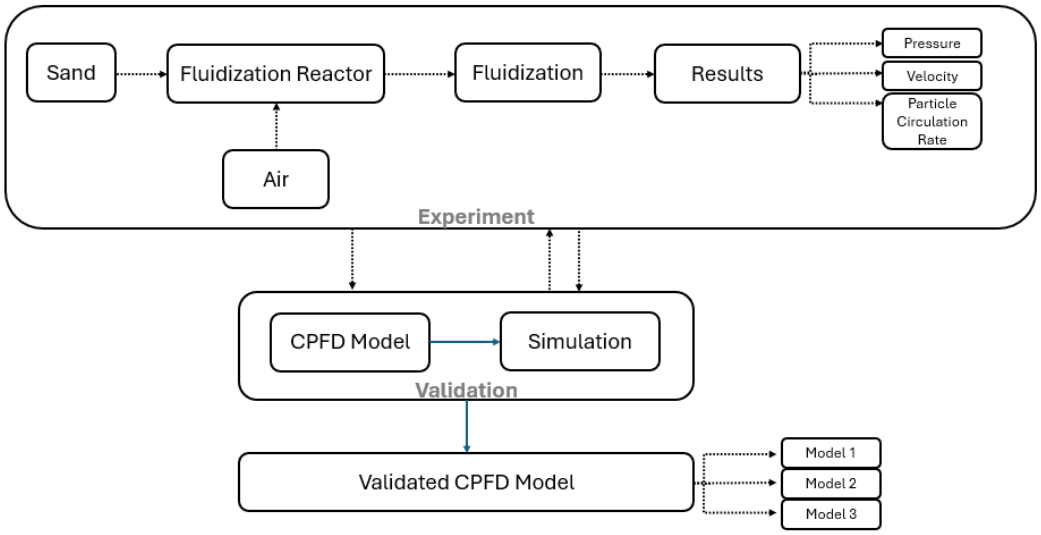

Figure 3.1 Methodology

The vibrating sieving machine were used to sieve the sand as shown in Figure 3.2. Different sieves sizes were selected to prepare the required sample. For the experimental work presented in this thesis, the sand particles ranged from 63-200 µm. After the sieving analysis, the sample was taken into a 50 ml beaker to calculate the void fraction.

Figure 3.2 Sieving Process

Figure 3.3 Void Fraction Calculation

3.1 Experimental Setup and Procedure

3.1.1 Equipment

The experimental setup utilized in this study comprises a 3D transparent cold bed column measuring 3 meters in height with a base diameter of 0.084 meters. Pressure transducers were interconnected with pressure tapping points positioned along the wall of the column and within the standpipe following the cyclone separator. The spacing between consecutive pressure points along the column height varies according to the configuration detailed in Figure 3.4. Compressed air at ambient condition was introduced through an air supply hose located at the column's base. The airflow from the compressor into the column was regulated by a control valve integrated into the rig. Figure 3.4 illustrates the schematic diagram depicting the locations of the pressure tapping points and air distributor along the column, while Figure 3.5 represents the experimental rig setup.

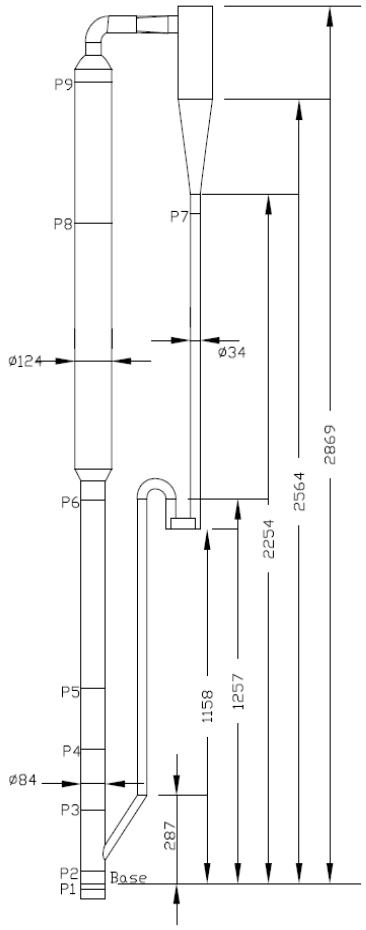

Figure 3.4 AutoCAD design of CFB

Figure 3.5 Experimental Setup of CFB

3.1.2 Procedure

The experiment was conducted within a circulating fluidized bed system comprising a riser, distributor, cyclone, standpipe and loop seal as shown in Figure 3.5. The riser had a height of 1316 mm and a diameter of 84 mm. A distributor pipe measuring 1300 mm in length and 124 mm in diameter was connected to the upper section of the riser, which then led to the cyclone via a lofted curved transition from circular to rectangular tubing. The cyclone had a diameter of 118 mm and a length of 305 mm. Additionally, an air flow distributor plate with dimensions of 84 × 34 mm was installed at the loop seal.

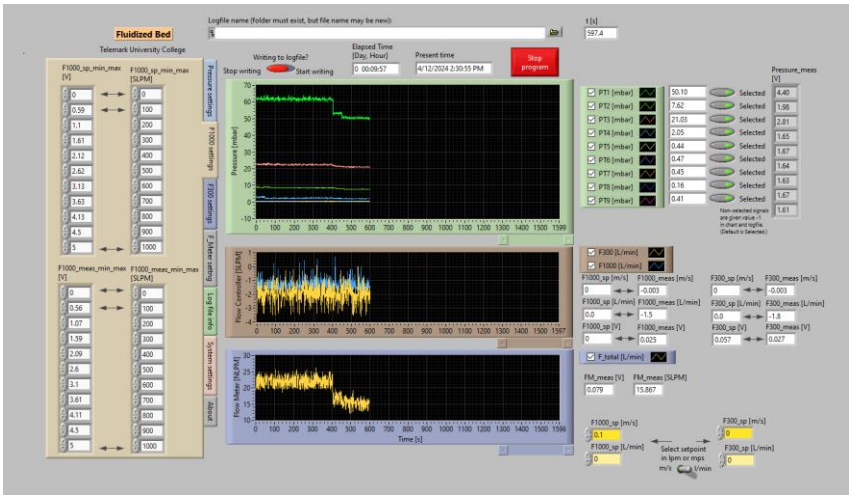

Figure 3.6 Pressure Data collection using LabVIEW.

Table 3.1 Pressure Transducers and their height from base

Pressure Transducers	Height from Base (mm)
P1	-20
P2	40
P3	240
P4	440
P5	640
P6	1255
P7	2190
P8	2160
P9	2620

Nine pressure transducers were attached to the wall of the CFB and LabVIEW was used to collect the data. The height of each pressure sensor is illustrated in Table 3.1. The air distributor at the bottom of the riser relates to the air supply and was controlled by the valve attached to the rig.

The sand particles of density 2650 kg/m^3 and mass of about 3.3 kg was filled into the riser (2.5 kg) and loop seal (0.8 kg) from the top of the riser and cyclone. Subsequently, with a specified bed height in both the riser and loop seal, compressed air was introduced and gradually increased until the circulation of bed materials was initiated. In line with circulating fluidized bed (CFB) principles, it was essential to maintain appropriate flow rates in both the riser and loop seal. The minimum required air flow rates were set at 650 SL/min for the riser and 12 SL/min for the loop seal.

Following the initiation of particle recirculation, some particles began escaping the system. To capture these escaping particles, a pipe was connected from the top of the cyclone to a bucket positioned on a weighing machine, as illustrated in Figure 3.7. The bucket on the weighing machine recorded the entrained mass readings, which were stored in a data file using Python software.

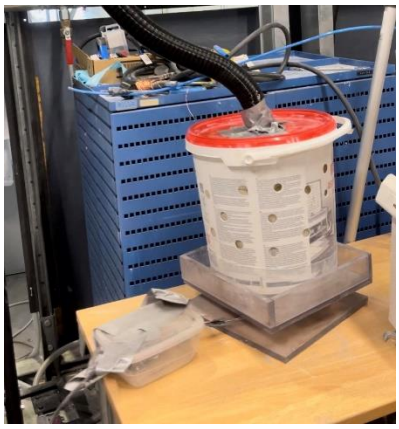

Figure 3.7 Collection of Elutriated Sand Particles

At the start of the experiment, data collection commenced after 2 minutes of circulation to ensure stable conditions for data acquisition. Subsequently, readings from LabVIEW were recorded over a span of 1 hour. These data sets were then utilized for validating the model in Barracuda VR.

Table 3.2 Bed Properties of Sand Particles

Sieve Range (μ m)	D, Mean Size (μ m)	Initial Weight (gm)	Final Weight (gm)	Particle Weight (gm)	Weight Fraction (W/T)	W/(T*D)
63-80	71.5	234.02	259.59	25.57	0.1236	0.0017
80-100	90	391.74	420.64	28.9	0.1397	0.0015
100-125	112.5	393.39	448.67	55.28	0.2672	0.0023
125-140	132.5	385.05	403.77	18.72	0.0905	0.0006
140-150	145	390.47	406.58	16.11	0.0778	0.0005
150-160	155	401.31	409.89	8.58	0.0414	0.0002
160-180	170	398.21	433.44	35.23	0.1703	0.0010
180-200	190	252.13	270.58	18.45	0.0891	0.0004
Total (T)				206.84	1	0.0086
Mean Particle Size (μ m) = (1/0.0086) = 116.059						

Table 3.3 Void Fraction and Mean Particle Diameter

Density	2650 kg/m^3
Bulk density	1405.54 kg/m^3
Solid void fraction	0.53
Mean Particle Diameter	116.05 μm

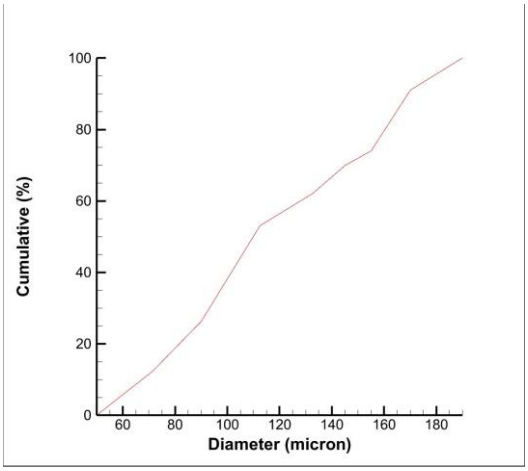

Figure 3.8 Particle Size Distribution

3.2 Simulation Set-up and Procedures

Particle fluid flow presents several difficulties, including intricate geometries, harsh operating environments and the requirement for a thorough investigation of bed interior properties. In contrast to experimental techniques, simulations provide a productive and cost-effective way

to handle these complexities within predetermined time limits. As a result, modeling was done using Computational Particle Fluid Dynamics (CPFD) software, Barracuda V.R to confirm experimental results and then guide design changes.

The simulation setup used in Barracuda to carry out the simulations is described in this chapter. Furthermore, the methods for verifying the CPFD model against experimental data are described in detail, including the actions done to guarantee the precision and dependability of the simulation results when compared to actual experimental data.

3.2.1 CAD Design and Simulation Set Up

After the measurement of physical CFB parameters, those dimensions were used to make the CAD model. The CAD model was made with the help of SOLIDWORKS 2020. After the completion of geometry, the CAD geometry from SOLIDWORKS was saved in STL format and was imported in Barracuda VR 2021. Uniform grid of total 80000 cells were established around the geometry for the simulations. The bottom of the geometry (riser and loop seal) were set up as inlet flow boundary condition while the top of the cyclone was considered as the pressure boundary condition.

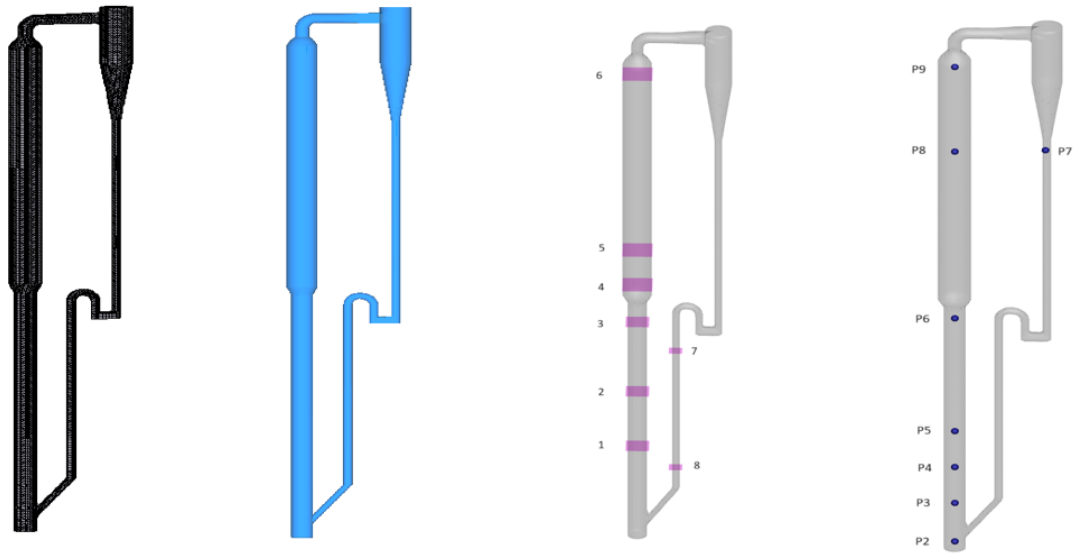

Figure 3.9 (a) Grid (b) CAD Geometry (c) Flux Planes (d) Pressure reading Points

The maximum momentum from redirection of particle collisions was assumed as 40 % and the normal to wall and tangential to wall collision were considered as the default value 0.85. The sand particles (SiO_2) were selected as the bed materials and air as the fluidizing gas at ambient temperature at 300 K. The Wen-Yu Ergun drag model was selected as the particles are in dense phase in riser and in dilute phase in distributor. Flux planes at different locations are shown in Figure 3.9 (c) and their height from base is shown in Table 3.4. To validate the pressure date

recorded in the experiment, exact locations of data points were given in the model as in Figure 3.9 (d) and Table 3.1.

Table 3.4 Height of Flux Planes from Base

S.N.	Height from Base (m)
First Flux Plane	0.5
Second Flux Plane	0.8
Third Flux Plane	1.2
Fourth Flux Plane	1.4
Fifth Flux Plane	1.6
Sixth Flux Plane	2.6
Seventh Flux Plane	1.06
Eighth Flux Plane	0.4

3.2.2 Governing Equation

The fluid phase mass and momentum conservation can be modelled by the volume averaged Navier-Stokes Equation and are used as a continuum on a Eulerian grid [18].

$$\frac{\partial(\theta_f \rho_f)}{\partial t} + \nabla.(\theta_f \rho_f u_f) = 0 \tag{3.1}$$

$$\frac{\partial(\theta_f \rho_f u_f)}{\partial t} + \nabla.(\theta_f \rho_f u_f) = \nabla p - F + \theta_f \rho_f g + \nabla.(\theta_f \tau_f) \tag{3.2}$$

$$F = \iint f m_s \left[D_s(u_f - u_s) - \frac{1}{\rho_s} \nabla p \right] dm_s du_s \tag{3.3}$$

Where θ_f, ρ_f, u_f, τ_f are fluid phase volume fraction, density, velocity and stress tensor and m_s, u_s are the mass and velocity of the particle. F is the total momentum exchange with particle phase per volume, g is the acceleration due to gravity and p is the pressure.

The solid phase can be modelled by a particle distribution function, Newtonian Equation of motion for each individual particle given by Equation 3.4. Considering the time rate of change of Equation 3.4 the Liouville Equation is obtained. This Equation assumes that there are no direct collisions or particle breakup.

$$f(x, m_s, u_s, t) dm_s du_s$$

$$\frac{\partial f}{\partial t} + \nabla_x.(f u_s) + \nabla u_s.(f A) = 0 \tag{3.4}$$

The particle acceleration, A as a function of aerodynamics drag, buoyancy, gravity and interparticle normal stresses can be expressed as Equation 3.5,

$$A = D_s(u_f - u_s) - \frac{1}{\rho_s}\nabla p + g - \frac{1}{\theta_s \rho_s}\nabla \tau_s \qquad 3.5$$

The particle volume fraction, θ_s and the particle stress τ_s, which are used to calculate the interparticle collisions and are expressed as Equation 3.7.

$$\theta_s = \iint f \frac{m_s}{\rho_s}\, dm_s du_s \qquad 3.6$$

$$\tau_s = \frac{10 P_s \theta_s^{\beta}}{max[(\theta_{cp} - \theta_s), \epsilon(1 - \theta_s)]} \qquad 3.7$$

Here, P_s, β, θ_{cp} are the constant term related with pressure, is a constant, particle volume fraction equals the close pack volume.

3.2.3 Drag Model

The major force associated with the particles is the fluid drag and can be written as:

$$F_P = m_s D(u_f - u_s) \qquad 3.8$$

m_s, D, u_f, u_s is the particle mass, drag function, fluid velocity and particle velocity. In Barracuda, numerous drag models are given and different drag models have their own features. The detailed information on various drag model is illustrated in Barracuda manual and can be extracted through Barracuda help menu bar[20]. As per the Bandara et al. [16], the Wen-Yu/Ergun drag model shows the best results since both dense and dilute phase are present in the system.

For the dilute system, the Wen-Yu drag model is used and is expressed as:

$$D_1 = \frac{3}{8} C_d \frac{\rho_f |u_f - u_s|}{r_s \rho_s} \qquad 3.9$$

where C_d is the drag coefficient and given as a function of the Reynolds number.

$$C_d = \begin{cases} \frac{24}{Re}\theta_f^{-2.65} & Re < 0.5 \\ \frac{24}{Re}\theta_f^{-2.65}(1 + 0.15Re^{0.687}) & 0.5 \le Re \le 1000 \\ 0.44\theta_f^{-2.65} & Re > 1000 \end{cases} \qquad 3.10$$

$$Re = \frac{2\rho_f r_s (u_f - u_s)}{\mu_f} \qquad 3.11$$

r_s, μ_f is the particle radius and fluid viscosity.

For the dense system, the Ergun drag model is considered,

$$D_2 = 0.5\left(\frac{180\theta_s}{\theta_s Re} + 2\right)\frac{\rho_f \left|u_f - u_s\right|}{r_s \rho_s} \qquad 3.12$$

The blended Wen-Yu/Ergun drag model can be expressed as:

$$D = \begin{cases} D_1 & \theta_s < 0.75\theta_{CP} \\ (D_2 - D_1)\left(\dfrac{\theta_s - 0.75\theta_{CP}}{0.85\theta_{CP} - 0.75\theta_{CP}}\right) & 0.75\theta_{CP} \geq \theta_s \geq 0.85\theta_{CP} \\ D_2 & \theta_s > 0.85\theta_{CP} \end{cases} \qquad 3.13$$

4 Result and Discussion

4.1 Model Validation

After importing the STL file in Barracuda and adding all the input and boundary conditions, the model was simulated according to different drag models and different grid sizes. The different models with different grid sizes were analyzed before finalizing the final drag model and grid size.

4.1.1 Drag Model Analysis

The experimental pressure data were analyzed along with simulations for the drag model analysis. The drag models Wen-Yu, Ergun and Wen-Yu Ergun were analyzed and Wen-Yu Ergun was used for all the simulations. The primary reason for selecting this model was based on experimental results from the pressure transducer and the specific characteristics of the system, which includes a dense phase in the riser and a dilute phase in the distributor. Additionally, the Wen-Yu Ergun model is well-documented in the literature for its accurate predictions in both dense and dilute phases.

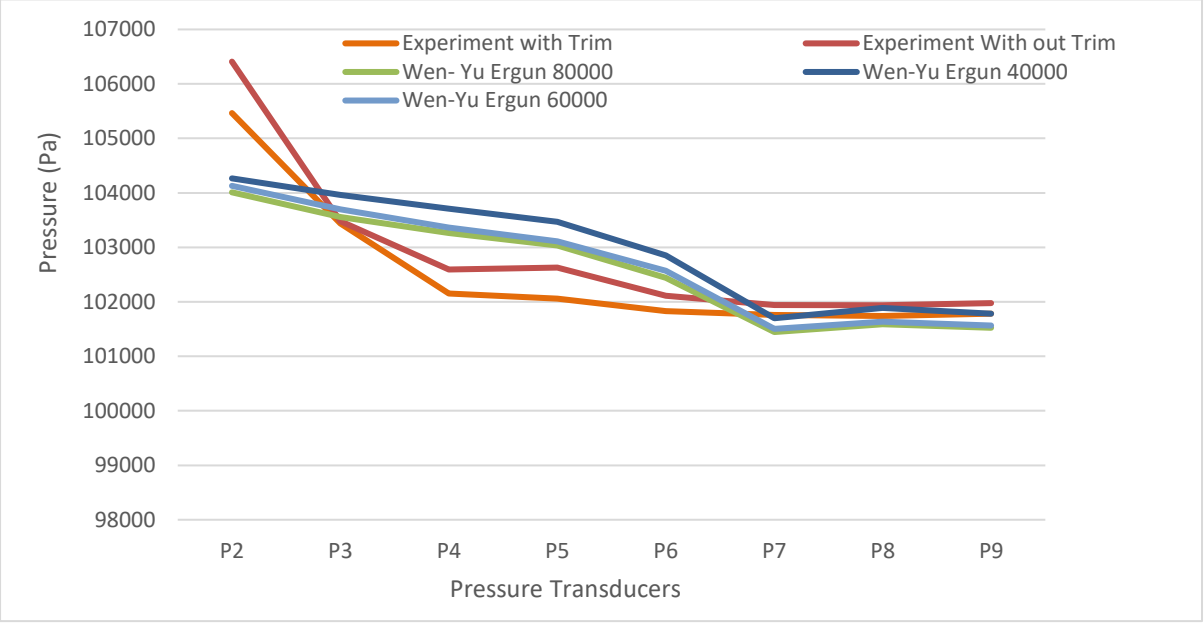

Figure 4.1 Pressure VS Pressure sensors with different grid numbers.

In Figure 4.1, two sets of experimental data are presented, one set without trim and the other with trim. The term “trim data” refers to the data collected after the initial 180 seconds of the experiment. Conversely, “without trim” data encompasses the measurements taken from the very beginning of the experiment and was taken for 3600 seconds..

4.1.2 Grid Sensitivity

The experimental pressure data were used for grid sensitivity analysis as shown in Figure 4.2. Grid 01, 02, 03, 04, 05, 06, 07, 08, 09,10 were constructed using uniform grid options. Grid 04 was constructed by refining the cell structure at the loop seal of grid 03.

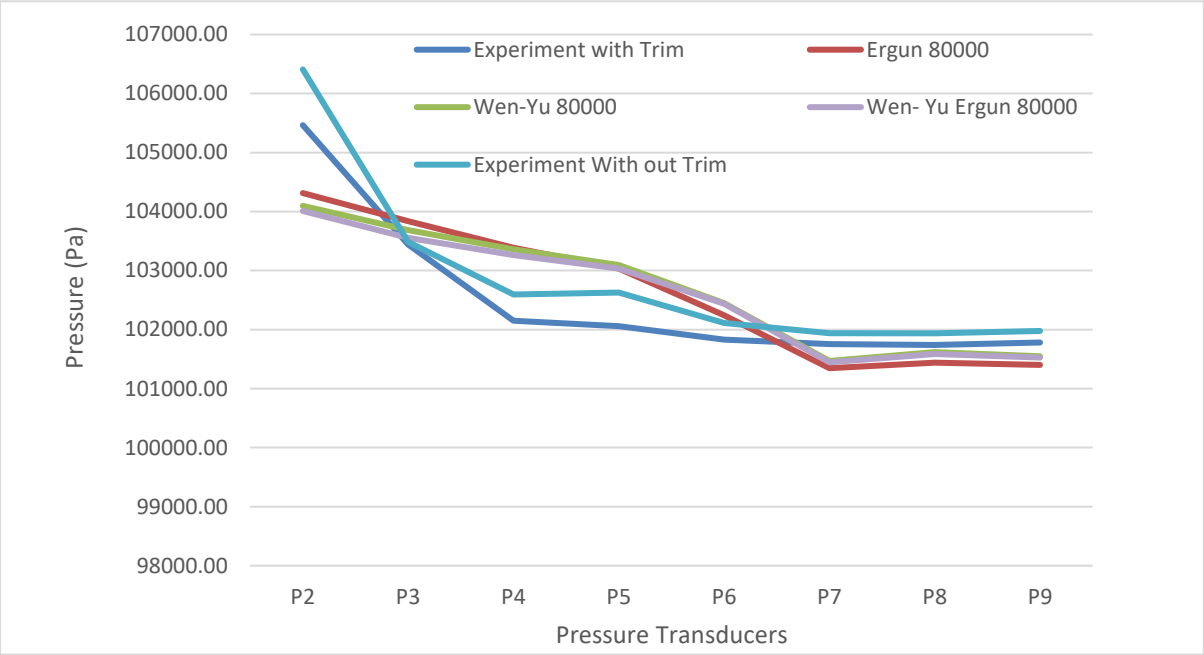

Figure 4.2 Pressure Vs Pressure Points with different drag model and same grid size

Table 4.1 Cells Vs Computational Particles

Grid	Cells	Computational Particles	Computational Particle to Cell Ratio
01	40000	35640	0.891
02	60000	56400	0.940
03	80000	77792	0.972
04	80000	77800	0.973
05	100000	96768	0.968
06	120000	111384	0.928
07	150000	139776	0.932
08	180000	167552	0.931
09	240000	235200	0.980
10	300000	285532	0.952

From Table 4.1, it clearly shows that increasing the cells size, number of computational particles size also increases. Cells were varied from 40000 to 300000 to see which computational model closely reflects the experimental model.

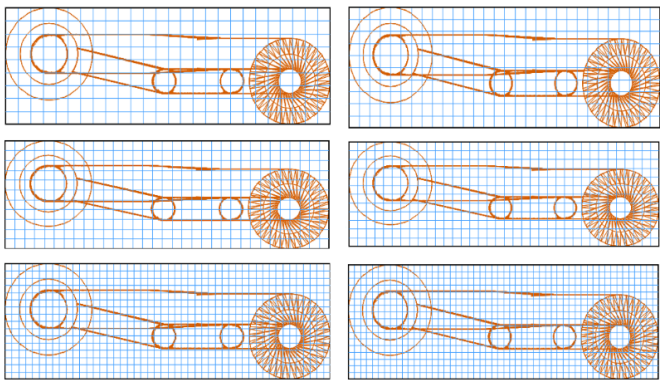

Figure 4.3 Grid size with (40, 60, 80, 120, 240, 300),000 uniform grid size (Top left to bottom right)

4.2 Impact of changing the diameter of Cyclone Keeping height constant:

The diameter of the cyclone was varied while keeping the height constant to investigate its impact on particle circulation rate. Adjusting the diameter of a cyclone separator in a circulating fluidized bed (CFB) yielded various outcomes in the particle circulation rate. Cyclone separators, used to remove particles from gases, have design parameters that significantly influence their efficiency. In the design consideration, with a height to diameter (H/D) ratio of 2.78, it was observed an increase in particle circulation rate of 1.6%.

Table 4.2 Varying Diameter keeping height of Cyclone constant

Height Constant		
H/D	Height (mm)	Diameter (mm)
2.28	305	133.77
2.38	305	128.15
2.48	305	122.98
2.58	305	118.21
2.68	305	113.80
2.78	305	109.71
2.88	305	105.90

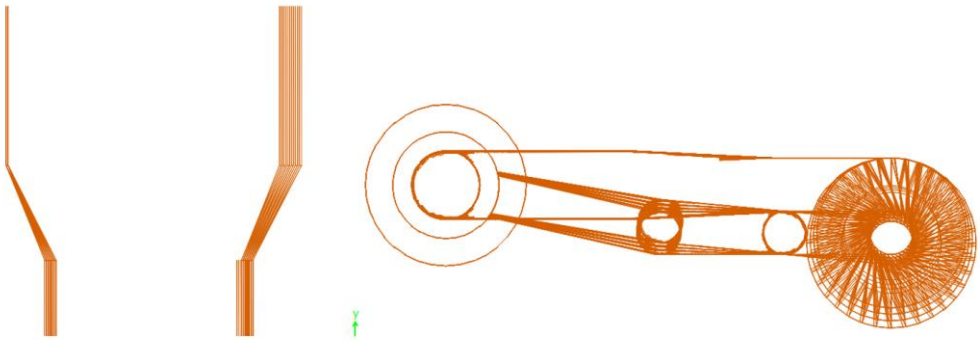

Figure 4.4 CAD model with varying diameter and constant height

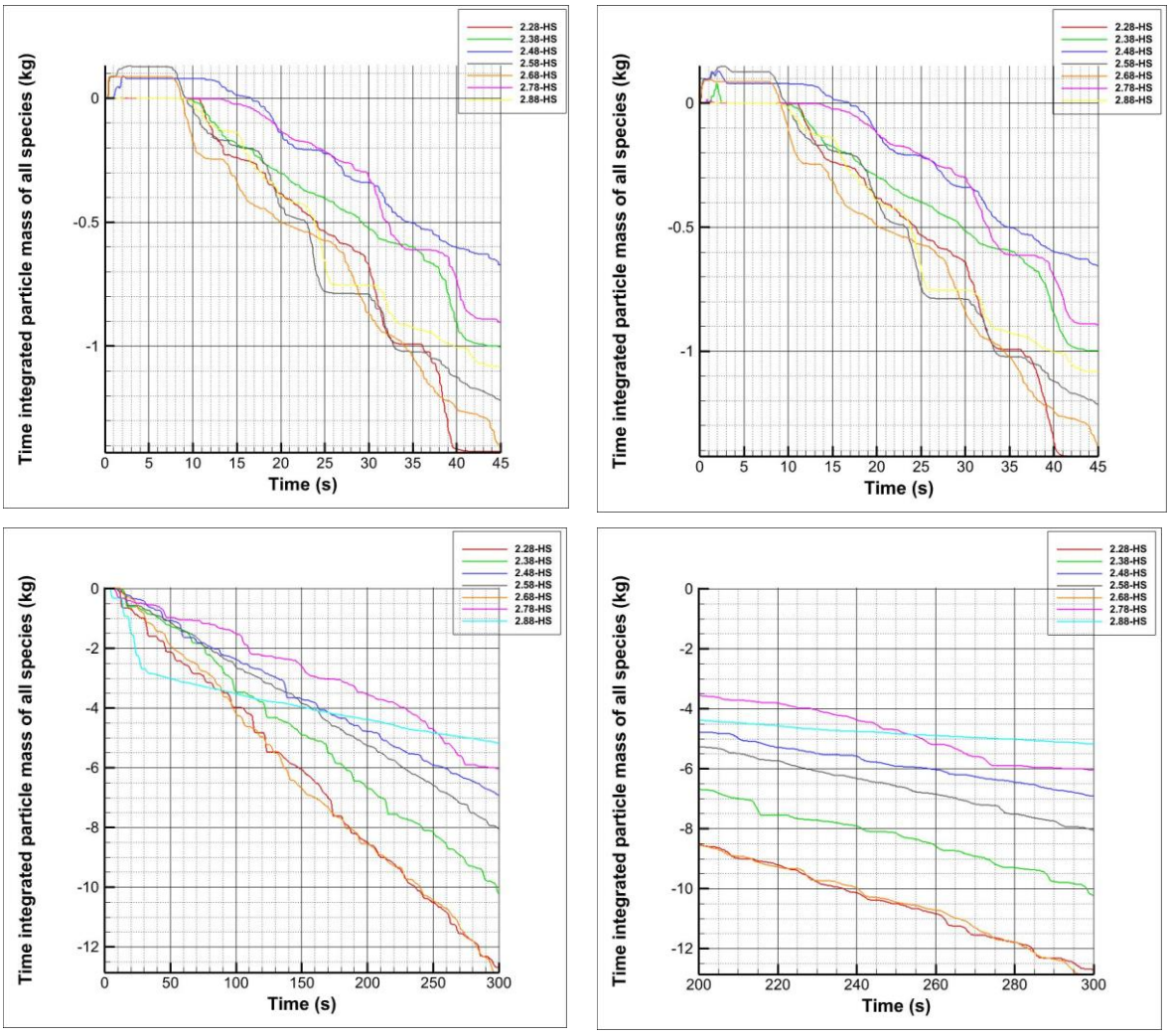

Figure 4.5 Time integrated particle mass of all species (kg), on Seventh and Eight plane (45 sec & 300 sec)

Typically, as the diameter increases, the particle circulation rate is expected to rise and then decrease beyond a certain point, following the formula

$$F_c = \frac{mv^2}{r}$$

However, in this case, the particles varied widely in size rather than being uniform. A diameter that works well for one particle size may not be suitable for others. For instance, a specific diameter may provide adequate centrifugal force for certain particles but may not be effective for others, leading to increased particle interactions and potential blockages in the standpipe. These blockages reduce the overall particle circulation rate.

The significance of uniform particle size on circulation rate is shown in Figure 4.6. In this study, all design parameters were maintained constant while varying the cyclone diameter, keeping the height constant. Notably, particles used were of a uniform size of 90 µm, as opposed to a heterogeneous particle size distribution. The results indicate that the particle circulation rate initially increases, reaches an optimal peak and subsequently declines. This behavior underscores the impact of particle size distribution on recirculation dynamics.

Table 4.3 Change of circulation rate at different H/D ratio

H/D	Circulation Rate (kg)	Change In Circulation Rate
2.28	1.02	-16.4
2.38	1.17	-4.1
2.48	0.8	-34.4
2.58	1.22	0.0
2.68	0.79	-35.2
2.78	1.24	1.6
2.88	0.75	-38.5

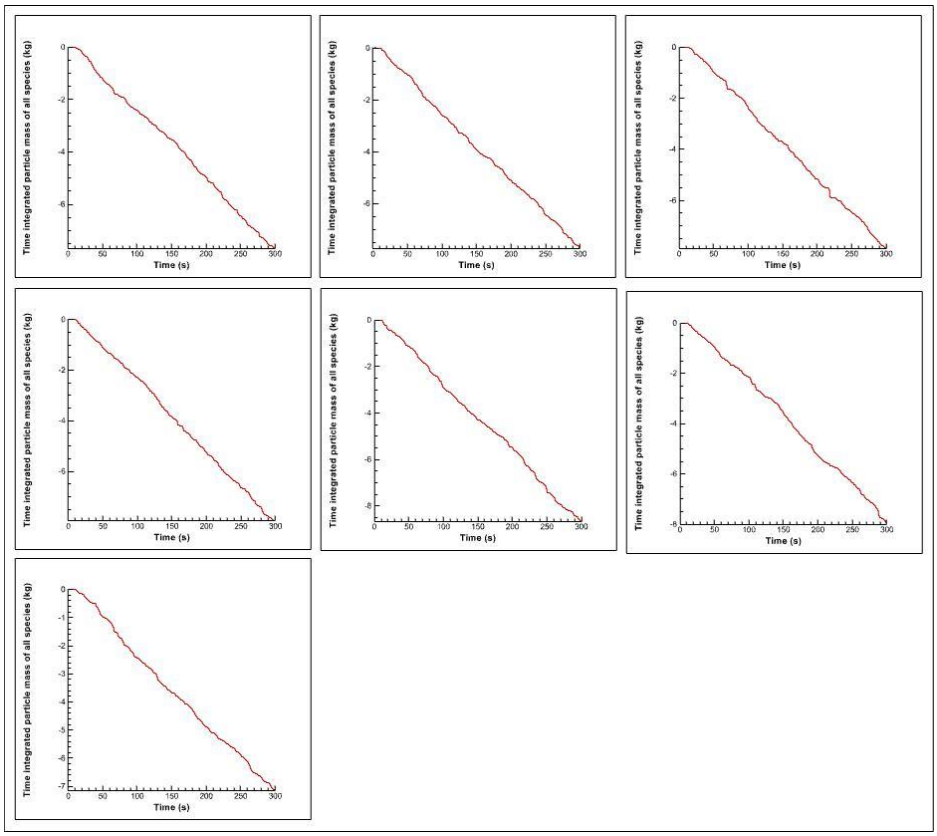

Figure 4.6 Time Integrated Particle Mass of All Species (Same particle size)

4.3 Impact of changing the height of cyclone keeping diameter constant:

Changing the height of a cyclone can have a direct impact on both gas and particle residence time. The longer the residence time, the more opportunity the particles have to be separated from the gas stream by centrifugal force. A taller cyclone can enhance both the separation efficiency and the rate of circulation as particles have more time to move towards the cyclone wall under the influence of centrifugal force.

In the design modification, with an H/D ratio of 2.68, as shown in Table 4.4 & 4.5, it was observed a 16.39% increase in the particle circulation rate. Several factors influence the particle circulation rate and a design optimized for a particular particle size may not be effective for a wide range of particle sizes.

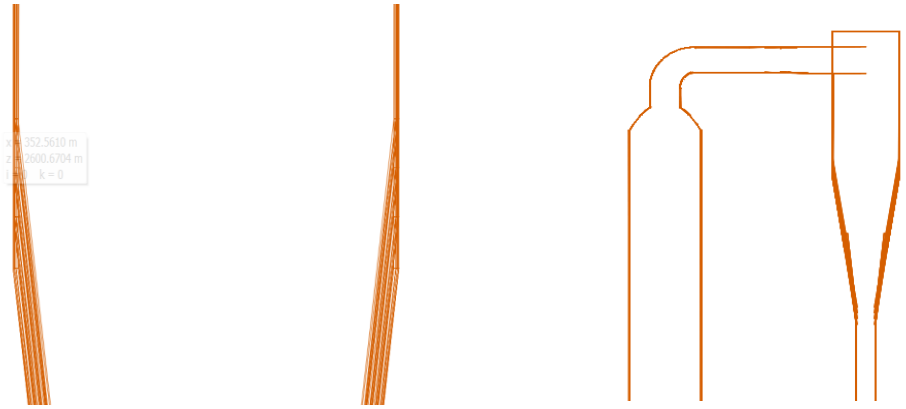

Figure 4.7 CAD model with constant diameter and varying height

Table 4.4 Varying height keeping Cyclone Diameter constant

Diameter Constant (118 mm)		
H/D	Diameter	Height
2.28	118	269.04
2.38	118	280.84
2.48	118	292.64
2.58	118	304.44
2.68	118	316.24
2.78	118	328.04
2.88	118	339.84

The height of the cyclone affects the velocity profile of the gas stream. A taller cyclone can maintain a stable and favorable velocity gradient for a specific particle size, enhancing separation efficiency for that size. However, this same velocity profile may negatively impact other particle sizes. For instance, while the increased residence time and centrifugal force may benefit some particles, they can lead to increased particle interactions and collisions for others. These interactions can cause particles to agglomerate and form blockages in the standpipe, which adversely affects the circulation rate.

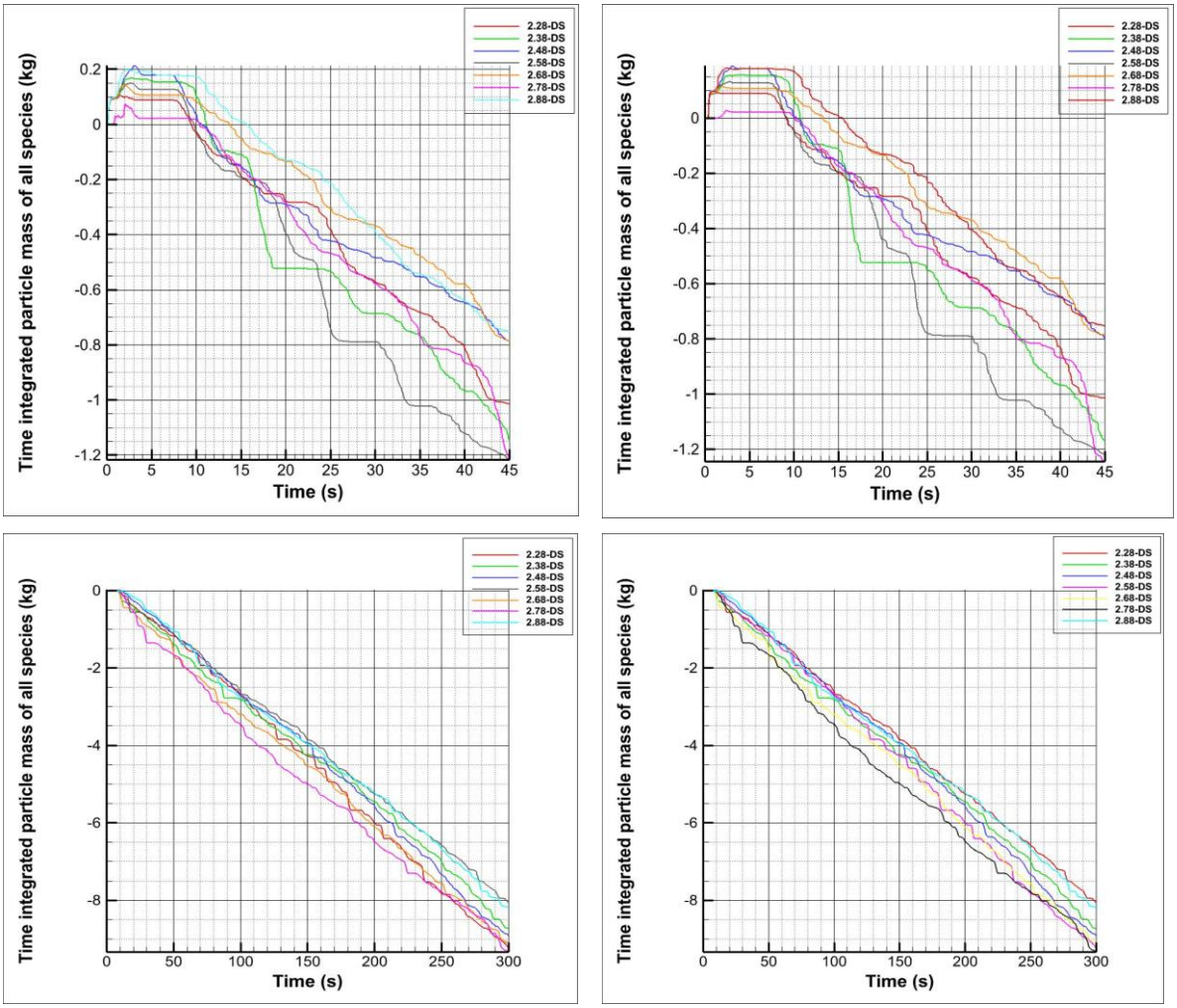

Figure 4.8 Particle circulation rate varying height keeping diameter same (Seventh and Eight Plane)

Table 4.5 Change of Circulation Rate varying height and constant cyclone diameter

H/D	Circulation Rate (kg)	Change In Circulation Rate
2.28	1.40	15.4
2.38	1	-18.03
2.48	0.65	-46.72
2.58	1.22	0.00
2.68	1.42	16.39
2.78	0.89	-27.05
2.88	1.08	-11.48

4.4 Impact of changing the angle of recirculation pipe (Return Leg /Downcomer)

The angle of the recirculation pipe significantly affects particle movement to the riser in a Circulating Fluidized Bed (CFB). Typically increasing the angle of the downcomer enhances gravitational forces, aiding particle movement. This improvement results in a higher particle recirculation rate as particles flow more smoothly and quickly to the riser. Additionally, the risk of blockage decreases with steeper angles as particles are more likely to settle and move smoothly within the downcomer.

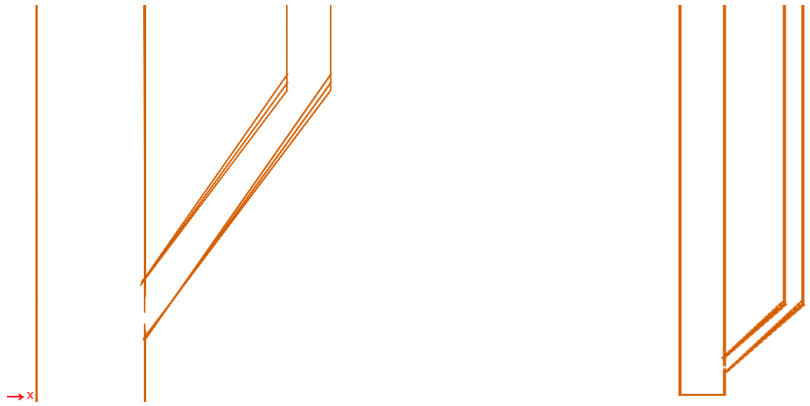

Figure 4.9 CAD model varying return circulation angle

To assess the impact on particle recirculation rate, 11 design variations were implemented, altering the angle from 52.27 degrees to 62.27 degrees. The angle of the return pipe used in the experiment was 57.27 degrees.

In the observations, the maximum circulation rate occurred at an angle of 52.27 degrees. Although this result appears unusual, it can be attributed to the backflow of particles from the riser to the loop seal, causing blockages and pushing particles backward towards the standpipe rather than the downcomer. As long as there is backpressure from particles inside the riser, the circulation rate will decrease. Therefore, the optimal angle was found to be 52.27 degrees, despite it being a shallower return angle.

Table 4.6 Change of circulation rate with respect to angle change

Angle	Circulation Rate (kg)	Change in Circulation Rate
52.27	1.6	31.15
53.27	1.42	16.39
54.27	1.3	6.56
55.27	1.12	-8.20
56.27	1.4	14.75
57.27	1.22	0.00
58.27	1.02	-16.39
59.27	1.14	-6.56
60.27	0.9	-26.23
61.27	1.13	-7.38
62.27	1.19	-2.46

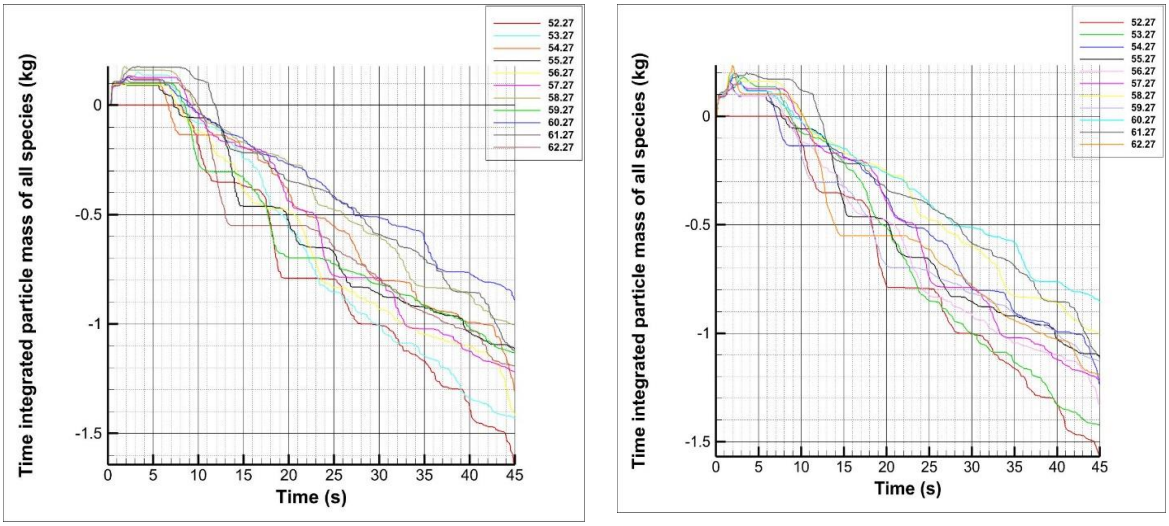

Figure 4.10 Time Integrated particle mass of all species (kg), varying return angle (Seventh and Eighth plane)

4.5 Impact of Changing the Height of Recirculation Pipe:

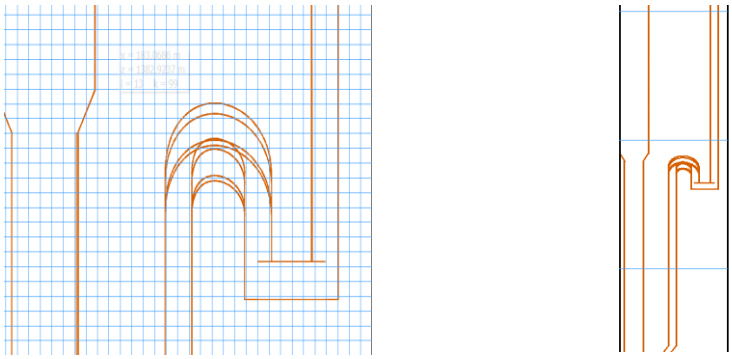

Figure 4.11 CAD model varying height of re-circulating pipe (Return leg)

Increasing the height of the downcomer or return pipe after the cyclone in a circulating fluidized bed (CFB) system can significantly impact the particle recirculation rate and the overall performance of the system. The height of the downcomer influences the gravitational forces acting on the particles, which affects their velocity and settling behavior. Specifically, an increased height necessitates that particles travel a longer vertical distance, influencing their dynamics within the system.

A taller downcomer results in a greater pressure drop, which can alter the flow dynamics of the particles. The velocity profile of the particles is also affected, higher height may lead to lower velocities if the system does not compensate for the increased gravitational and pressure drop effects. This adjustment is critical as improper height can hinder the effective recirculation of particles.

In the design considerations, nine modifications were made, varying the recirculating height from 950 mm to 990 mm. The original height of the recirculating pipe in the experiment was 970 mm. Varying the recirculating height also influences the height just after the loop seal. A greater height requires more pressure to transfer sand to the riser, while a lesser height facilitates more particle flow from the riser to the loop seal. Therefore, maintaining an appropriate height is a challenging yet crucial task. If the height is too low, particles circulate but not optimally, as some pressure is pushing particles from the loop seal towards the standpipe.

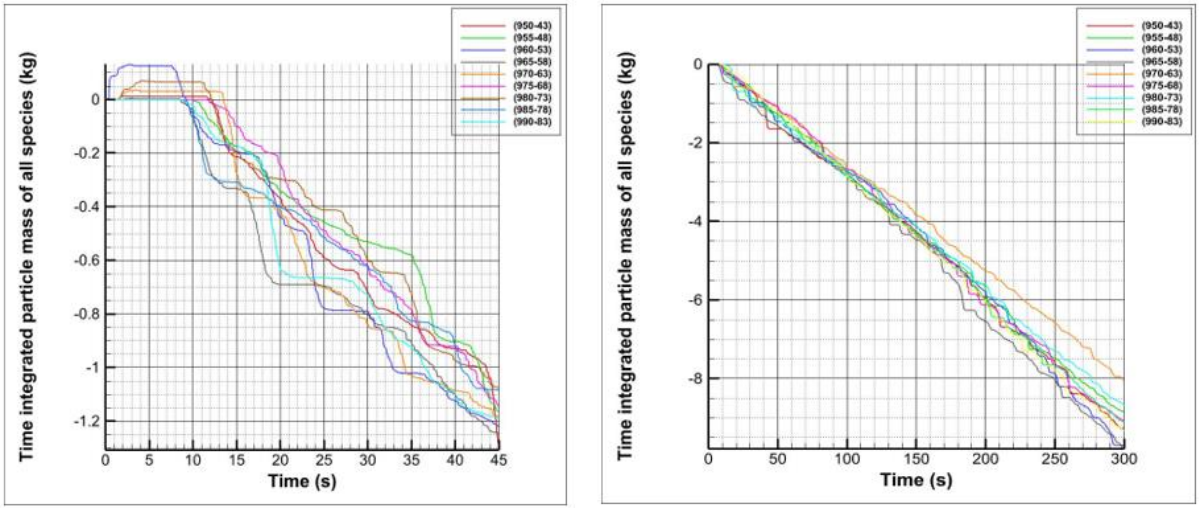

Figure 4.12 Time Integrated particle mass of all species (kg), varying recirculating pipe length (45 & 300 sec)

In the nine simulations, it was observed that the configuration with a height of 965 mm and a height of 58 mm just after loop seal achieved the maximum recirculation rate. Initially, until 45 seconds, the circulation rate was highest for the configuration with a height of 950 mm. However, when extending the simulation to 300 seconds, the (965-58) mm configuration consistently provided a better circulation rate.

Table 4.7 Change of Circulation rate with respect to length and height of recirculating pipe

Length and Height of Recirculating Pipe		
Height (mm)	Circulation Rate (kg)	Change in Circulation Rate
(950-43)	1.31	7.38
(955-48)	1.16	-4.92
(960-53)	1.2	-1.64
(965-58)	1.26	3.28
(970-63)	1.22	0.00
(975-68)	1.15	-5.74
(980-73)	1.08	-11.48
(985-78)	1.1	-9.84
(990-83)	1.08	-11.48

4.6 Impact of Change of Angle Between Riser and Distributor

Altering the angle between the riser and distributor significantly impacts the particle recirculation rate. A smaller angle improves the circulation rate, whereas increasing the angle reduces the gas velocity at the junction, leading to particle accumulation at the joint instead of their ascent to the cyclone. Consequently, a larger angle results in decreased circulation.

Table 4.8 Change in radius of distributor, changing angle between riser and distributor

a (mm)	b (mm)	c (mm)	d (mm)	e (degree)
58.37	43.22	42	40	112.25
59.19	43.54	42	40	113.25
60.02	43.87	42	40	114.25
60.87	44.23	42	40	115.25
61.73	44.61	42	40	116.25
62.61	44.99	42	40	117.25
63.51	45.71	42	40	118.25
64.41	45.85	42	40	119.25
65.33	46.31	42	40	120.25
66.28	46.79	42	40	121.25
67.24	47.31	42	40	122.25
68.23	47.83	42	40	123.25
69.24	48.39	42	40	124.25

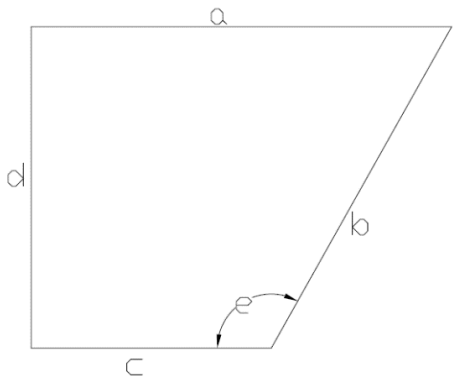

Figure 4.13 Riser and Distributor

The angle between the riser and distributor is typically adjusted to ensure that only specific particles reach the cyclone, while others are excluded. If there are no requirements for particle collection or segregation within the riser, a standard riser design can be employed.

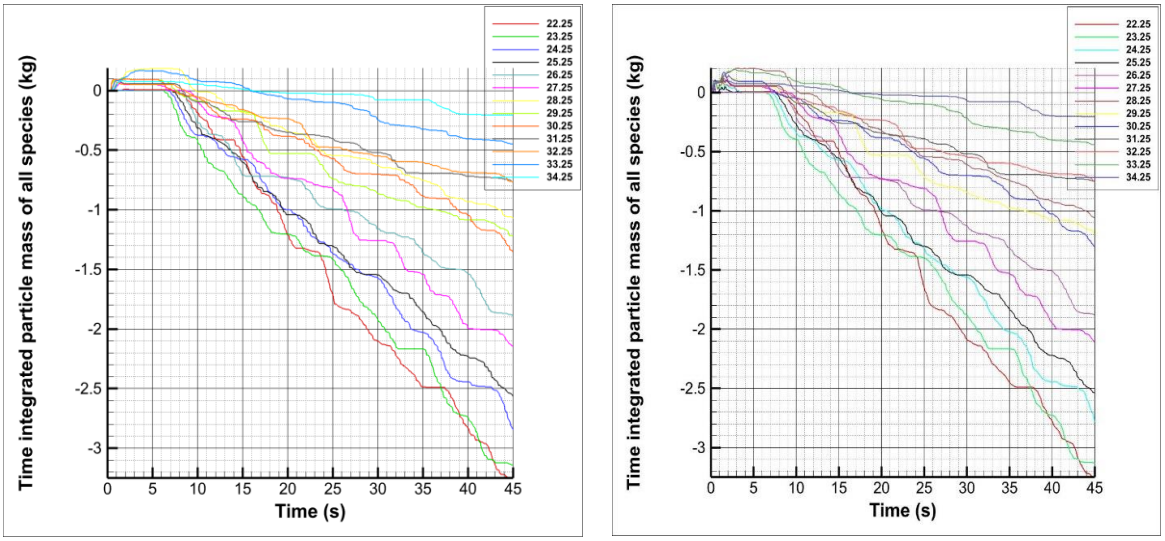

Figure 4.14 Time Integrated mass of all species (kg) varying angle between riser and distributor (Seventh and Eighth plane)

In the design considerations, thirteen design changes were implemented, varying the angle from 22.25 degrees to 34.25 degrees. Consistent with expectations, the recirculation rate is maximized at an angle of 22.25 degrees.

4.7 Impact of Changing double riser to a single riser Model

In the initial experimental model, the riser had a diameter of 84 mm and the distributor had a diameter of 124 mm. The mass of sand in the riser was 2.8 kg, with a height of 37.5 cm. To evaluate the recirculation rate, the distributor was replaced creating a single riser model. Two different configurations were tested, in one the mass of sand in the riser remained constant, and in the other the height of the sand was kept constant. Both models were tested individually to observe the particle circulation rate.

As the base diameter changed from 84 mm to 124 mm, the base area also changed, affecting the inlet velocity. In the experimental case, the inlet velocity decreased from 1.954 m/s to 1.279 m/s with the change in diameter. From Figure 4.16, it is evident that as the velocity increases, the particle circulation rate also increases.

In the subsequent diagrams, the volume of sand was kept constant, and the initial 37.5 cm sand height was reduced to 25.40 cm due to the increased diameter. The results clearly show that lower velocity results in a lower circulation rate. Also, the particle accumulation on double riser model and single riser model is shown in Figure 4.15.

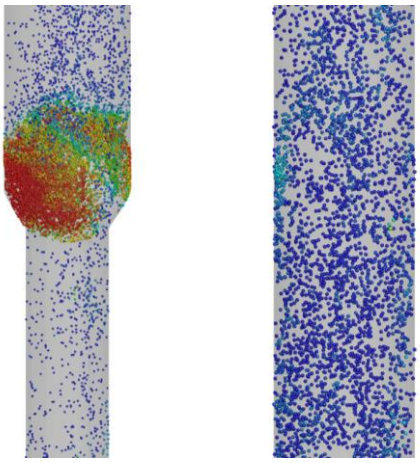

Figure 4.15 Double riser and Single riser (Left & Right)

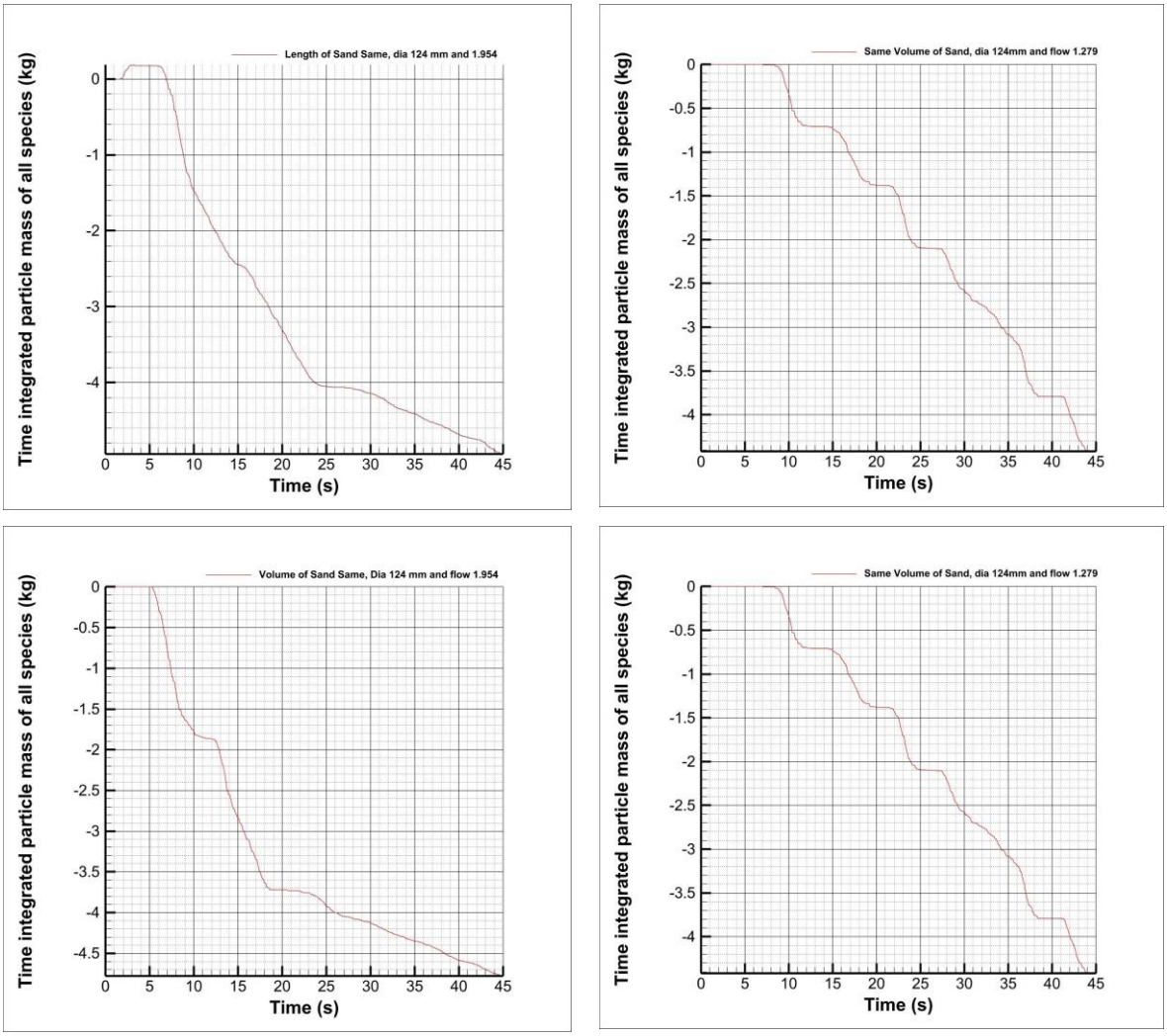

Figure 4.16 Time Integrated Particle mass of all species (kg) changing double riser to a single riser

The key point to note is that simply adding more sand does not necessarily increase circulation. Factors such as particle to particle, particle to wall collisions and an improper velocity profile due to large particle accumulation can also disrupt the circulation rate. Therefore, maintaining an appropriate mass of sand is crucial for achieving a good recirculation rate.

4.8 Final Design Modifications and Simulation Overview

A series of design modifications were done to optimize particle circulation. Specific changes include recirculating pipe angle, length of recirculating pipe, cyclone diameter and height.

These modifications were individually optimized through simulations and a final design was created incorporating the most efficient one from each individual design change. This final configuration was then subjected to comprehensive simulations to evaluate its performance.

The final cyclone design was simulated over two distinct time intervals: 45 seconds and 300 seconds. The simulations revealed the following increased recirculation rates.

45 seconds: 32.7%

300 seconds: 20.40%

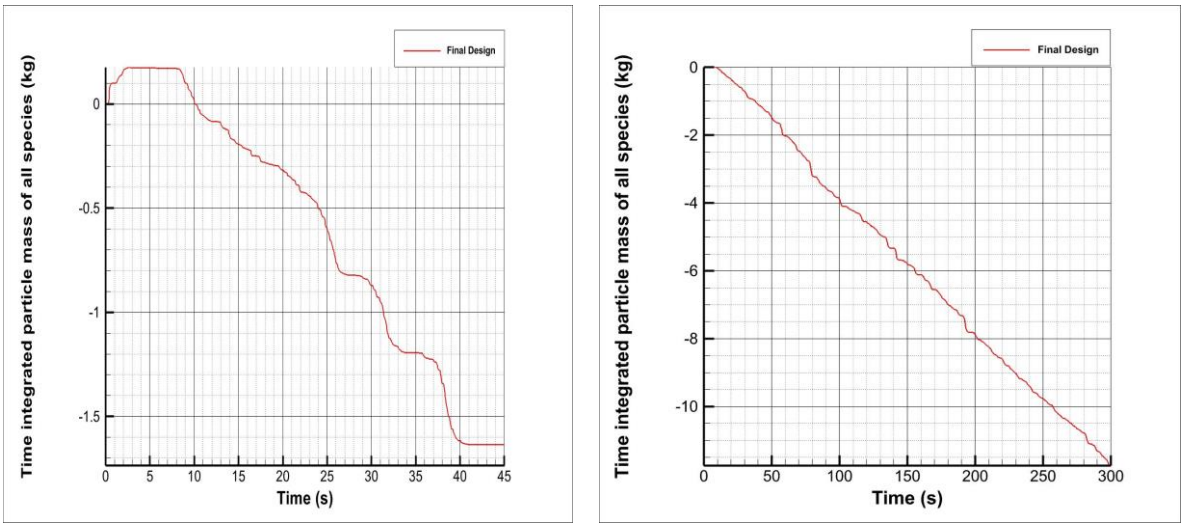

Figure 4.17 Particle circulation rate on Final Design (45 & 300 sec)

The higher recirculation rate at 45 seconds can be attributed to the initial presence of sand in the standpipe, which provided an immediate boost in circulation efficiency. As the system reached a steady state, the percentage increase in recirculation rate decreased, stabilizing at a lower rate. The enhanced circulation in the final design is primarily due to several factors like optimized flow dynamics, reduced particle wall collisions and particle to particle collisions.

The simulations did not exhibit a low high low graph trend for particle circulation rates. This consistency is likely due to the use of particles with a size distribution range rather than uniform particle sizes.

5 Conclusion

This thesis investigates the hydrodynamic flow behavior of Geldart A and Geldart B particles within a cold circulating fluidized bed. The experimental setup utilized a mixture of Geldart A and Geldart B particles ranging from 63-200 μm in size and having a density of 2650 kg/m^3. The pneumatic conveying air flow velocities for the riser and loop seal were determined and pressure transducer data at different locations of the experimental rig were collected using LabVIEW. A CPFD model was developed using Barracuda VR 2021, and the CAD design was created with SolidWorks 2020. The experimental and computational models were validated using pressure data obtained from transducers positioned at different locations on the experimental rig. Various drag models and grid sizes were examined to validate the model. Based on simulation results and literature review, the Wen-Yu Ergun drag model with 80,000 cell and uniform grid size was selected for the final model.

The minimum riser and loop seal aeration rates were found to be 650 SL/min and 12 SL/min, respectively. The inlet velocity of the riser was increased incrementally by 50 SL/min, starting from 50 SL/min, until particles began to move from the riser to the cyclone. Upon reaching the cyclone, the loop seal aeration was increased by 2 SL/min increments until particles began flowing from the loop seal to the riser, stabilizing at a final flow rate of 12 SL/min.

In simulations, grid size was refined to create a finer uniform grid, but this resulted in greater deviations due to the grid size becoming smaller than the particle size. The deviations between the experimental and computational pressure data ranged from a maximum of 2.4% to a minimum of 0.09%.

Following the validation of the computational model, various design modifications were made to the circulating fluidized bed including changes to the cyclone diameter and height, recirculating angle, recirculating height and the angle between the riser and distributor. Results showed that varying the cyclone diameter with an H/D ratio of 2.78 increased particle circulation rate by 1.6% and varying the cyclone height with an H/D ratio of 2.68 increased the rate by 16.39%. Changing the return leg angle from 57.27 degrees to 52.27 degrees resulted in a 31.15% increase in particle circulation rate, while reducing the return leg height from 970 mm to 965 mm increased the rate by 3.28%. Additionally, adjusting the angle between the riser and distributor demonstrated that a smaller angle improved circulation and reduced particle accumulation in this region. Comparing single and double riser models (both 124 mm in diameter) revealed that the single riser model significantly improved circulation rate due to reduced particle accumulation between risers. However, in systems where certain particle's entry into the cyclone is restricted, the double riser model is found to be more effective.

The final computational model, optimized for maximum circulation rate from individual design adjustments demonstrated a 20.40 % increase in particle circulation rate. This study underscores the importance of various factors influencing particle circulation rate, including particle density, shape, size and the design parameters of the circulating fluidized bed (CFB). The results indicate that particle circulation does not follow a simple linear or low-high-low pattern due to the wide range of particle sizes used in both experiments and simulations. Therefore, it is crucial to understand the impact of design parameters on particle circulation

rate before establishing new gasification plant as a plant optimized for one type of particle may not be suitable for a broad range of particles.

6 References

[1] Moradi, A., Samani, N. A., Mojarrad, M., Sharfuddin, M., Bandara, J. C., & Moldestad, B. M. E. (2020). Experimental and computational studies of circulating fluidized bed. International Journal of Energy Production and Management, 5(4), 302–313. https://doi.org/10.2495/EQ-V5-N4-302-313

[2] Dell'Orco, S., Rizzo, A. M., Buffi, M., & Chiaramonti, D. (2018). Design of a circulating fluidized bed combustor for lignin-Rich residue derived from second-Generation bioethanol production plant. Chemical Engineering Transactions, 65, 277–282. https://doi.org/10.3303/CET1865047

[3] Slivka, R. M., Chinn, M. S., & Grunden, A. M. (2011). Gasification and synthesis gas fermentation: An alternative route to biofuel production. In Biofuels (Vol. 2, Issue 4, pp. 405–419). https://doi.org/10.4155/bfs.11.108

[4] Dechsiri, C. (2004). Particle transport in fluidized beds : experiments and stochastic models. s.n.].

[5] A. R. Abrahamsen and D. Geldart, 'Behaviour of gas-fluidized beds of fine powders part I. Homogeneous expansion', *Powder Technology*, vol. 26, no. 1, pp. 35–46, May 1980, doi: 10.1016/0032-5910(80)85005-4.

[6] *A STUDY OF THE DESIGN OF FLUIDIZED BED REACTORS FOR BIOMASS GAS IFICATION Ajmal LatifMEng*. (1999).

[7] R. K. Niven, 'Physical insight into the Ergun and Wen & Yu Equations for fluid flow in packed and fluidised beds', *Chemical Engineering Science*, vol. 57, no. 3, pp. 527–534, Feb. 2002, doi: 10.1016/S0009-2509(01)00371-2.

[8] B. Leckner, 'Hundred years of fluidization for the conversion of solid fuels', *Powder Technology*, vol. 411, p. 117935, Oct. 2022, doi: 10.1016/j.powtec.2022.117935.

[9] D. Kunii and O. Levenspiel, *Fluidization engineering*, 2. ed., Reprinted. in Butterworth-Heinemann series in chemical engineering. Amsterdam Heidelberg: Elsevier ; Butterworth-Heinemann, 2012.

[10] B. M. So, H. M. Abdelmotalib, M. Y. Hashim, and I.-T. Im, 'Computational study on heat transfer and bed flow according to different regimes of fluidized beds', *J Mech Sci Technol*, vol. 33, no. 12, pp. 5881–5887, Dec. 2019, doi: 10.1007/s12206-019-1133-0.

[11] D. Geldart, 'Types of gas fluidization', *Powder Technology*, vol. 7, no. 5, pp. 285–292, 1973, doi: https://doi.org/10.1016/0032-5910(73)80037-3.

[12] A. Anantharaman, R. A. Cocco, and J. W. Chew, 'Evaluation of correlations for minimum fluidization velocity (*Umf*) in gas-solid fluidization', *Powder Technology*, vol. 323, pp. 454–485, Jan. 2018, doi: 10.1016/j.powtec.2017.10.016.

[13] R. Jaiswal, B. M. E. Moldestad, M. S. Eikeland, H. K. Nielsen, and R. K. Thapa, 'Image Processing and Measurement of the Bubble Properties in a Bubbling Fluidized Bed Reactor', *18*, 2022, doi: 10.3390/en15217828.

[14] R. Jaiswal, C. E. Agu, R. K. Thapa, and B. M. E. Moldestad, 'Study of fluidized bed regimes using Computational Particle Fluid Dynamics', presented at the The 59th Conference on Simulation and Modelling (SIMS 59), 26-28 September 2018, Oslo Metropolitan University, Norway, Nov. 2018, pp. 271–276. doi: 10.3384/ecp18153271.

[15] University College of South East Norway, kjølnes ring 56, 3901, Porsgrunn, Norway and R. K. Thapa, 'Flow Regime Identification in a Fluidized Bed Combustion Reactor', *IJMO*, vol. 6, no. 3, pp. 188–194, Jun. 2016, doi: 10.7763/IJMO.2016.V6.525.

[16] J. C. Bandara, R. Thapa, H. K. Nielsen, B. M. E. Moldestad, and M. S. Eikeland, 'Circulating fluidized bed reactors – part 01: analyzing the effect of particle modelling parameters in computational particle fluid dynamic (CPFD) simulation with experimental validation', *Particulate Science and Technology*, vol. 39, no. 2, pp. 223–236, Feb. 2021, doi: 10.1080/02726351.2019.1697773.

[17] A. Moradi, N. A. Samani, M. Mojarrad, M. Sharfuddin, J. C. Bandara, and B. M. E. Moldestad, 'Experimental and computational studies of circulating fluidized bed', *Int. J. EQ*, vol. 5, no. 4, pp. 302–313, Nov. 2020, doi: 10.2495/EQ-V5-N4-302-313.

[18] D. M. Snider, 'An Incompressible Three-Dimensional Multiphase Particle-in-Cell Model for Dense Particle Flows', *Journal of Computational Physics*, vol. 170, no. 2, pp. 523–549, Jul. 2001, doi: 10.1006/jcph.2001.6747.

[19] P. J. O'Rourke and D. M. Snider, 'A new blended acceleration model for the particle contact forces induced by an interstitial fluid in dense particle/fluid flows', *Powder Technology*, vol. 256, pp. 39–51, Apr. 2014, doi: 10.1016/j.powtec.2014.01.084.

[20] *CPFD Software. LLC, "Barracuda VR Series 2021," User Manual.*

[21] R. K. Niven, 'Physical insight into the Ergun and Wen & Yu Equations for fluid flow in packed and fluidised beds', *Chemical Engineering Science*, vol. 57, no. 3, pp. 527–534, Feb. 2002, doi: 10.1016/S0009-2509(01)00371-2.

[22] Soomro, A., Samo, S. R., & Hussain, A. (2012). Fluidization in cold flow circulating fluidized bed system. In Energy, Environment and Sustainable Development (pp. 161–173). Springer-Verlag Vienna. https://doi.org/10.1007/978-3-7091-0109-4_17

[23] Yu, X., Blanco, P. H., Makkawi, Y., & Bridgwater, A. v. (n.d.). *CFD and experimental studies on a circulating fluidised bed reactor for biomass gasification*.

[24] Song, C., Pei, B., Jiang, M., Wang, B., Xu, D., & Chen, Y. (2016). Numerical analysis of forces exerted on particles in cyclone separators. *Powder Technology*, *294*, 437–448. https://doi.org/10.1016/j.powtec.2016.02.052

[25] U. Muschelknautz, E. Muschelknautz *Separation Efficiency of Recirculating Cyclones in Circulating Fluidized Bed*.

[26] R. K. Niven, ‘Physical insight into the Ergun and Wen & Yu Equations for fluid flow in packed and fluidised beds’, Chemical Engineering Science, vol. 57, no. 3, pp. 527–534, Feb. 2002, doi: 10.1016/S0009-2509(01)00371-2.

[27] Bridgwater, A. v. (1995). The technical and economic feasibility of biomass gasification for power generation. In Fuel (Vol. 14, Issue 5).

[28] Leva, M. , Fluidization, McGraw-Hill Book Company, Inc., New York, 1959

[29] B. Waldie, Growth mechanism and the dependence of granule size on drop size in fluidized-bed granulation, Chemical Engineering Science, Volume 46, Issue 11, 1991.

[30] Huang, Y. (n.d.). Dynamic model of circulating fluidized bed. https://researchrepository.wvu.edu/etd/2749

[31] Xie, J., W. Zhong, B. Jin, Y. Shao and Y. Huang (2013). "Eulerian–Lagrangian method for three-dimensional simulation of fluidized bed coal gasification." Advanced Powder Technology 24(1): 382-392.

[32] Snider, D. M. (2001). "An Incompressible Three-Dimensional Multiphase Particle-in-Cell Model for Dense Particle Flows." Journal of Computational Physics 170(2): 523-549.

[33] Andrews, M. J. and P. J. O'Rourke (1996). "The multiphase particle-in-cell (MP-PIC) method for dense particulate flows." International Journal of Multiphase Flow 22(2): 379-402.

[34] J. R. Grace, A. A. Avidan, and T. M. Knowlton, Eds., *Circulating Fluidized Beds*. Dordrecht: Springer Netherlands, 1996. doi: 10.1007/978-94-009-0095-0.

7 Appendices

Appendix A

Pressure Variation vs grid size and drag model

	P2	P3	P4	P5	P6	P7	P8	P9
Experiment with Trim	105464.8242	103439.725	102151.4646	102058.4246	101832.2738	101756.6556	101740.2716	101781.9332
Ergun 80000	104313.64	103839.03	103389.72	103032.60	102244.09	101346.27	101440.05	101404.28
Wen-Yu 80000	104097.255	103683.4823	103357.6285	103093.2504	102448.0078	101469.0682	101618.8432	101550.375
Wen- Yu Ergun 80000	104009.9815	103556.8607	103262.7537	103034.8887	102439.9565	101445.6608	101586.9875	101526.1635
Ergun 120000	112191.0935	111848.8863	111577.1765	111330.8762	110687.389	109580.199	109852.6673	109774.2187
Wen-Yu 120000	115076.6749	114789.7999	114562.9968	114375.0668	113927.677	112774.9564	113104.6168	113004.627
Wen-Yu Ergun 120000	114165.5804	113903.481	113692.0134	113494.8633	112964.3757	111813.4203	112175.2225	112067.6829
Ergun 150000	104261.6636	103897.5764	103571.5551	103320.4765	102659.5372	101533.8259	101723.3277	101671.8123
Wen-Yu 150000	106687.1328	106317.2397	106076.5609	105874.865	105385.5964	104295.198	104646.6658	104560.8463
Wen-Yu Ergun 150000	106894.4783	106522.7093	106290.3102	106098.0093	105600.6829	104494.5809	104846.1685	104770.6205
Wen-Yu Ergun 0.53 100000	108319.3011	107970.6848	107709.782	107462.8309	107028.9555	105575.4522	106012.1447	105921.3561
Experiment With out Trim	106409.251	103483.4969	102594.0121	102626.99	102112.0239	101939.8033	101937.0781	101976.2271
Wen-Yu Ergun 80000 refined	103991.5169	103629.7692	103346.9847	103103.3614	102501.972	101455.3504	101606.6286	101541.2669
Wen-Yu Ergun 0.53 80000	104481.614	103927.6985	103546.9792	103214.0735	102585.3314	101468.0448	101615.168	101550.438
Wen-Yu Ergun 300000	115423.0373	115008.802	114640.4973	114349.0634	113737.067	112752.5546	113002.3459	112945.5474
Wen-Yu Ergun 60000	104128.8019	103695.2964	103365.9911	103110.9674	102571.7419	101503.5782	101634.1453	101564.8293
Wen-Yu Ergun 40000	104266.021	103963.5231	103710.6355	103470.3073	102849.2375	101698.8927	101885.2414	101783.786
Wen-Yu Ergun 100000	107828.9611	107567.2343	107389.2533	107189.8253	106749.975	105503.809	105896.3438	105795.7217
Wen-Yu Ergun 180000	106262.3185	105946.0406	105724.633	105546.8231	105091.4639	103939.1312	104251.883	104180.0196
Wen-Yu Ergun 240000	106435.9681	106123.5991	105897.2029	105704.6849	105175.8195	104163.7514	104414.4561	104337.9969

Appendix B

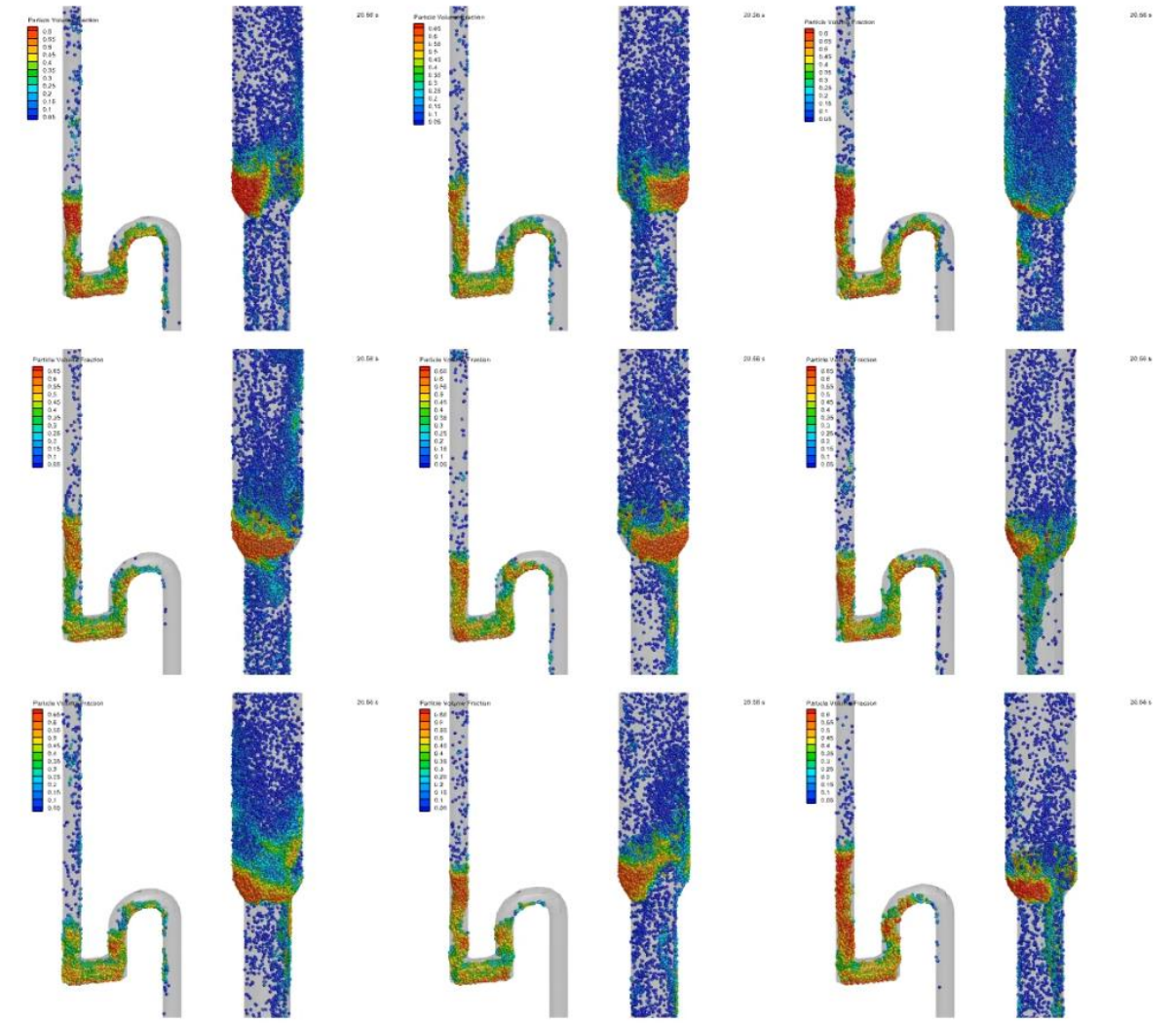

Particle Volume fraction Varying height of Recirculating pipe

Appendix C

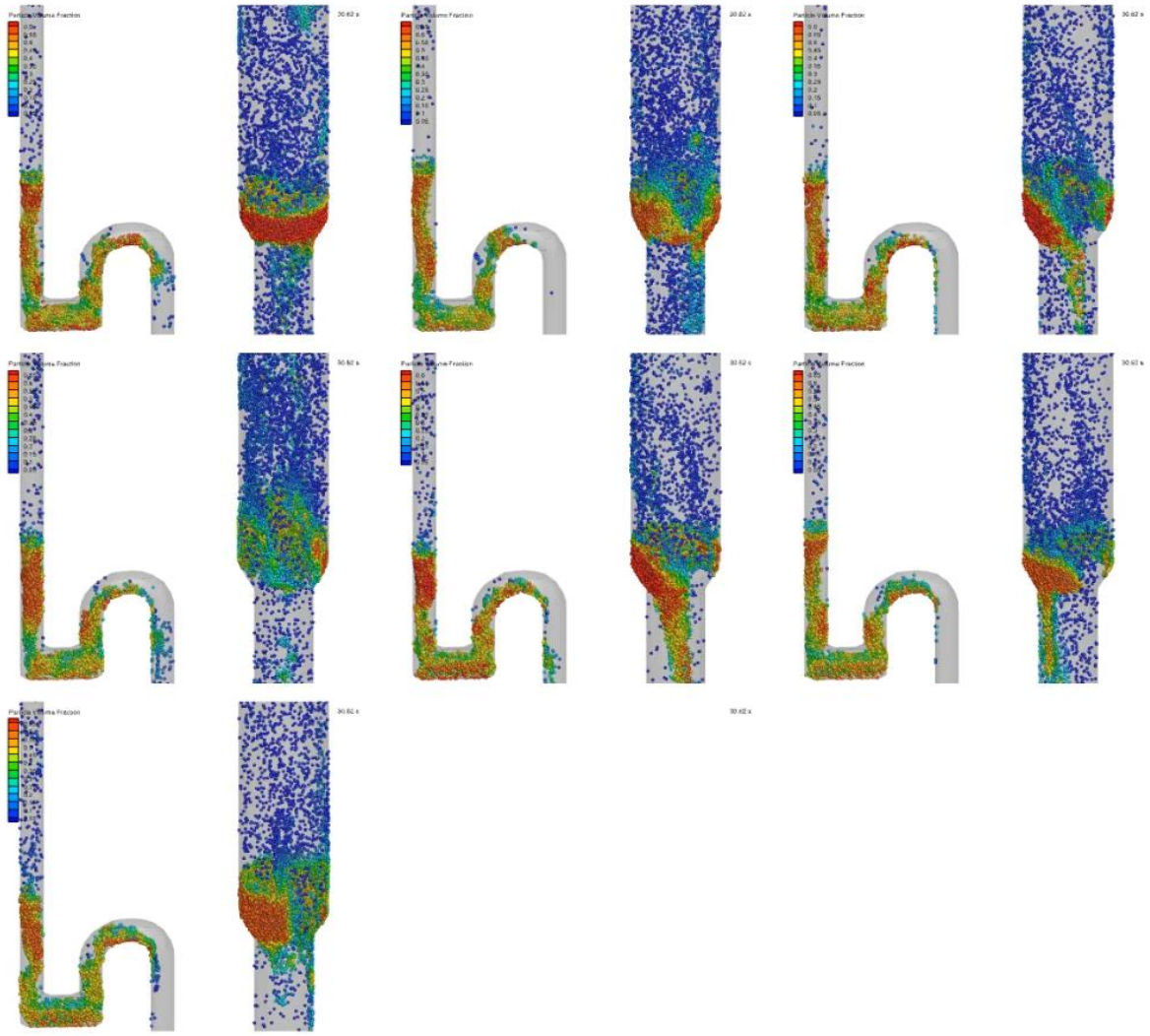

Particle Volume fraction Varying diameter of Cyclone and 90 µm sand diameter.

University of South-Eastern Norway

Faculty of Technology, Natural Sciences and Maritime Sciences, Campus Porsgrunn

FMH606 Master's Thesis

Title: Experimental and computational studies to investigate flow dynamics of Geldart A and Geldart B particles in a Circulating Fluidized Bed (CFB)

USN supervisor: Professor Britt Margrethe Emilie Moldestad, Rajan Jaiswal (PhD)

External partner: Kathmandu University, Nepal

Task background:

Fluidized bed typically circulating fluidized bed is an efficient technology widely used in various industrial processes, such as combustion, gasification, and chemical production. CFB systems provide enhanced heat transfer by enhancing gas solid contact time, fuel flexibility, and reduced emissions, making them crucial in the transition to sustainable energy solutions. In a Circulating Fluidized Bed (CFB), different regimes refer to distinct operational states characterized by the behavior of particles and gas within the bed. For the specified bed inventory and particle, the CFB system undergoes transitions between these regimes depending on various factors, such as gas velocity. The primary regimes in a CFB are bubbling, fast fluidization or turbulent, and pneumatic conveying regime.

This master thesis project will investigate flow dynamics in a Circulating Fluidized Bed (CFB) reactor, specifically using Geldart A and B particles. The objective is to enhance the understanding of the dynamics and behaviors of Geldart A particles within a CFB reactor for improved operational efficiency and applications. Understanding the behaviour of Geldart A and Geldart B particles is crucial in designing and operating a CFB system. This work will employ experimental and CFD methods to investigate flow dynamics in the circulating fluidized bed, contributing to a comprehensive understanding of particle behavior in CFB systems.

Task description:

Objective

The major objective of this project work is to investigate the flow dynamics of the binary mixture of the particles in a Circulating Fluidized Bed.
The following experimental and simulation tasks will be carried out to accomplish the objectives:

Experimental tasks

- Experiments on the CFB at different gas velocities
- Characterization of the particles used.
- Record the entrained mass of the particle during one hour of the test.
- Record the change in pressure along the reactor during fluidization in a LabView.

Simulation tasks

- Develop a CAD model of the experimental CFB setup available at USN.
- Develop a CPFD model of the CFB using the Barracuda Virtual Reactor software and validate the CPFD model against the experimental data.
- Investigate the influence of design parameters on the particle circulation rate and fluid dynamics behaviour.
- Develop a final design incorporation all the best part design from individual design modifications.
- Post-processing of the CPFD model results to identify:
  - Rapid fluidization regime and distribution of particles in the bed.
  - Particle circulation.
  - Pneumatic conveying rate of the particles.
  - Flow dynamics behaviour of the CFB at different operating conditions.

Student category: (EET or PT students)

The task is suitable for online students (not present at the campus): No

Practical arrangements:
Experimental works will be carried out on a circulating fluidized bed reactor located at USN, Porsgrunn Campus. A CPFD simulation software, Barracuda, will be available for a certain period.

Supervision:
As a general rule, the student is entitled to 15-20 hours of supervision. This includes the necessary time for the supervisor to prepare for supervision meetings (reading material to be discussed, etc).

Signatures:

Supervisor : 01.03.2024

Student : Subham Kandel

Student : 01.03.2024